INTERNATIONAL JOURNAL OF
ROBOTICS AND AUTOMATION (IJRA)

INTERNATIONAL JOURNAL OF ROBOTICS AND AUTOMATION (IJRA)

VOLUME 4, ISSUE 1, 2013

EDITED BY
DR. NABEEL TAHIR

INTERNATIONAL JOURNAL OF ROBOTICS AND AUTOMATION (IJRA)

CSC Publishers, 2013

EDITORIAL PREFACE

Robots are becoming part of people's everyday social lives - and will increasingly become so. In future years, robots may become caretaking assistants for the elderly or academic tutors for our children, or medical assistants, day care assistants, or psychological counselors. Robots may become our co-workers in factories and offices, or maids in our homes. It is the *First* Issue of Volume *Four* of International Journal of Robotics and Automation (IJRA). IJRA published six times in a year and it is being peer reviewed to very high International standards.

The initial efforts helped to shape the editorial policy and to sharpen the focus of the journal. Started with Volume 4, 2013, IJRA appears with more focused issues. Besides normal publications, IJRA intends to organize special issues on more focused topics. Each special issue will have a designated editor (editors) – either member of the editorial board or another recognized specialist in the respective field.

IJRA looks to the different aspects like sensors in robot, control systems, manipulators, power supplies and software. IJRA is aiming to push the frontier of robotics into a new dimension, in which motion and intelligence play equally important roles. IJRA scope includes systems, dynamics, control, simulation, automation engineering, robotics programming, software and hardware designing for robots, artificial intelligence in robotics and automation, industrial robots, automation, manufacturing, and social implications etc. IJRA cover the all aspect relating to the robots and automation.

The IJRA is a refereed journal aims in providing a platform to researchers, scientists, engineers and practitioners throughout the world to publish the latest achievement, future challenges and exciting applications of intelligent and autonomous robots. IJRA open access publications have greatly speeded the pace of development in the robotics and automation field. IJRA objective is to publish articles that are not only technically proficient but also contains state of the art ideas and problems for international readership.

In order to position IJRA as one of the top International journal in robotics, a group of highly valuable and senior International scholars are serving its Editorial Board who ensures that each issue must publish qualitative research articles from International research communities relevant to signal processing fields.

IJRA editors understand that how much it is important for authors and researchers to have their work published with a minimum delay after submission of their papers. They also strongly believe that the direct communication between the editors and authors are important for the welfare, quality and wellbeing of the Journal and its readers. Therefore, all activities from paper submission to paper publication are controlled through electronic systems that include electronic submission, editorial panel and review system that ensures rapid decision with least delays in the publication processes.

To build its international reputation, we are disseminating the publication information through Google Books, Google Scholar, Directory of Open Access Journals (DOAJ), Open J Gate, ScientificCommons, Docstoc and many more. Our International Editors are working on establishing ISI listing and a good impact factor for IJRA. We would like to remind you that the success of our journal depends directly on the number of quality articles submitted for review. Accordingly, we would like to request your participation by submitting quality manuscripts for review and encouraging your colleagues to submit quality manuscripts for review. One of the great benefits we can provide to our prospective authors is the mentoring nature of our review process. IJRA provides authors with high quality, helpful reviews that are shaped to assist authors in improving their manuscripts.

Editorial Board Members
International Journal of Robotics and Automation (IJRA)

Editorial Board

TABLE OF CONTENTS

Pages

Designing SDRE-Based Controller for a Class of Nonlinear Singularly Perturbed Systems

Seyed Mostafa Ghadami   *m.gadami@srbiau.ac.ir*
Department of Electrical Engineering,
Science and Research Branch,
Islamic Azad University, Tehran, Iran

Roya Amjadifard   *amjadifard@tmu.ac.ir*
Assistant Professor,
Kharazmi University,
Tehran, Iran

Hamid Khaloozadeh   *h_khaloozadeh@kntu.ac.ir*
Professor,
K.N. Toosi University of Technology,
Tehran, Iran

Abstract

Designing a controller for nonlinear systems is difficult to be applied. Thus, it is usually based on a linearization around their equilibrium points. The state dependent Riccati equation control approach is an optimization method that has the simplicity of the classical linear quadratic control method. On the other hand, the singular perturbation theory is used for the decomposition of a high-order system into two lower-order systems. In this study, the finite-horizon optimization of a class of nonlinear singularly perturbed systems based on the singular perturbation theory and the state dependent Riccati equation technique together is addressed. In the proposed method, first, the Hamiltonian equations are described as a state-dependent Hamiltonian matrix, from which, the reduced-order subsystems are obtained. Then, these subsystems are converted into outer-layer, initial layer correction and final layer correction equations, from which, the separated state dependent Riccati equations are derived. The optimal control law is, then, obtained by computing the Riccati matrices.

Keywords: Singularly Perturbed Systems, State-Dependent Riccati Equation, Nonlinear Optimal Control, Finite-Horizon Optimization Problem, Single Link Flexible Joint Robot Manipulator.

---

1. INTRODUCTION

Designing regulator systems is an important class of optimal control problems in which optimal control law leads to the Hamilton-Jacobi-Belman (HJB) equation. Various techniques have been suggested to solve this equation. One of these techniques, which are used for optimizing in infinite horizon, is based on the state-dependent Riccati equation (SDRE). In this technique, unlike linearization methods, a description of the system as state-dependent coefficients (SDCs) and in the form $f(x)=A(x)x$ must be provided. In this representation, $A(x)$ is not unique. Therefore, the solutions of the SDRE would be dependent on the choice of matrix $A(x)$. With suitable choice of the matrix, the solution to the equation is optimal; otherwise, the equation has suboptimal solutions. Bank and Mhana [1] proposed a suitable method for the selection of SDCs. Çimen [2] provided the condition for the solvability and local asymptotic stability of the SDRE closed-loop system for a class of nonlinear systems. Khaloozadeh and Abdolahi converted the nonlinear regulation [3] and tracking [4] problems in the finite-horizon to a state-dependent quasi-Riccati equation. They also provided an iterative method based on the Piccard theorem, which obtains a solution at a low convergence rate but good precision. On the other hand, the system discussed in this study is a class of nonlinear singularly perturbed systems. Naidu and Calise [5] dealt with

the use of the singular perturbation theory and the two time scale (TTS) method in satellite and interplanetary trajectories, missiles, launch vehicles and hypersonic flight, space robotics. For LTI singularly perturbed systems, Su et al. [6] and Gajic et al. [7] performed the exact slow-fast decomposition of the linear quadratic (LQ) singularly perturbed optimal control problem in infinite horizon by deriving separate Riccati equations. Also, Gajic et al. [8] did the same for the case of finite horizon. Amjadifard et al. [9, 10] addressed the robust disturbance attenuation of a class of nonlinear singularly perturbed systems and robust regulation of a class of nonlinear singularly perturbed systems [11], and also position and velocity control of a flexible joint robot manipulator via fuzzy controller based on singular perturbation analysis [12]. Fridman [13, 14] dealt with the infinite horizon nonlinear quadratic optimal control problem for a class of non-standard nonlinear singularly perturbed systems by invariant manifolds of the Hamiltonian system and its decomposition into linear-algebraic Riccati equations.

In this study, we extend results of [13, 14] to the finite horizon by slow-fast manifolds of the Hamiltonian system and its decomposition into SDREs. Our contribution is that, we used the singular perturbation theory and SDRE method together. In the proposed method, first, the state-dependent Hamiltonian matrix is derived for the system under study. Then, this matrix is separated into the reduced-order slow and fast subsystems. Using the singular perturbation theory, the state equations and SDREs are converted into outer layer, initial layer correction and final layer correction equations, which are then solved to obtain the optimal control law. The block diagram of the proposed method is shown in Figure 1.
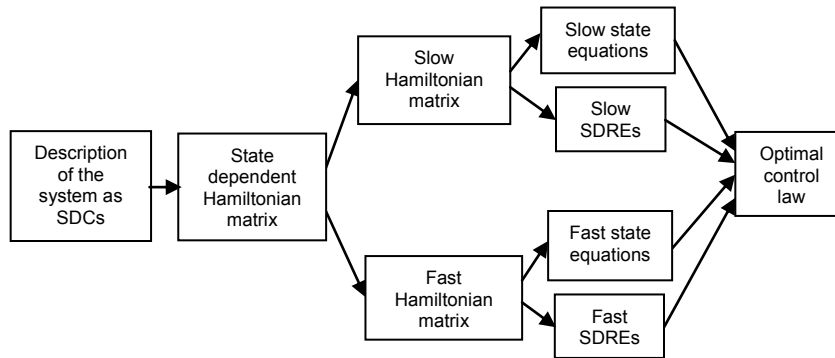
FIGURE 1: The design procedure stages in the proposed method.

The remainder of this study is organized as follows. Section 2 explains the structure of the singularly perturbed system for optimization. Section 3 involves in the description of steps of the design procedure in the proposed method. Section 4 presents the simulation results of the system used in the proposed method. Finally, the study culminates with indication of remarks in section 5.

2. PROBLEM FORMULATION

The following nonlinear singularly perturbed system is assumed:

$$E\dot{x} = f(x) + B(x)u, x(t_0) = x_0, \tag{1}$$

where $x(t) = \begin{bmatrix} x_1 \\ x_2 \end{bmatrix}, x_i \in R^{n_i}, i = 1,2$ are the states of system, and $x=0_n$ is the equilibrium point of the

system ($n=n_1+n_2$). This system is full state observable, autonomous, nonlinear in the states, and affine in the input. Moreover, $f(x) = \begin{bmatrix} f_1(x_1,x_2) \\ f_2(x_1,x_2) \end{bmatrix}, f_i \in R^{n_i}, B(x) = \begin{bmatrix} B_1(x_1,x_2) \\ B_2(x_1,x_2) \end{bmatrix}, B_i \in R^{n_i}, i = 1,2$

are differentiable with respect to x_1, x_2 for a sufficient number of times. Furthermore, $f(0_n)=0_n$,

Seyed Mostafa Ghadami, Roya Amjadifard & Hamid Khaloozadeh

$B(x)\neq 0_{n\times m}$, $\forall x \in R^n$ and $E = \begin{bmatrix} I_{n_1\times n_1} & 0_{n_1\times n_2} \\ 0_{n_2\times n_1} & \varepsilon I_{n_2\times n_2} \end{bmatrix}$ that $\varepsilon>0$ is a small parameter. Provided these, it is desired to obtain the optimal control law $u(x)\in R^m$ such that for $k(x)\in R^n$, $k(0_n)=0_n$ and pointwise positive definite matrix $R(x)\in R^n\rightarrow R^{m\times m}$, the following performance index J is minimized.

$$J = h(x(t_F)) + \int_{t_0}^{t_F} \left(k^T(x)k(x) + u^T R(x)u\right)dt \tag{2}$$

Suppose that $k(x)$, $R(x)$ are differentiable with respect to x_1, x_2 for a sufficient number of times. Moreover, t_F is chosen such that it is sufficiently large with respect to the dominant time constant of the slow subsystem, and $x(t_F)$ is free.

3. THE PROPOSED METHOD

The singularly perturbed system (1) with performance index (2) is assumed. Defining the co-state vector $\lambda(x) = \begin{bmatrix} \lambda_1(x_1,x_2) \\ \lambda_2(x_1,x_2) \end{bmatrix}$, $\lambda_i \in R^{n_i}$, $i = 1,2$, the Hamiltonian function is obtained as (3):

$$H(x,u,\lambda) = \frac{1}{2}k^T(x)k(x) + \frac{1}{2}u^T R(x)u + \lambda_1^T(f_1(x_1,x_2) + B_1(x_1,x_2)u) + \lambda_2^T(f_2(x_1,x_2) + B_2(x_1,x_2)u). \tag{3}$$

According to the optimal control theory, the necessary conditions for optimization would be as follow [2]:

$$\dot{x}_1 = (\frac{\partial H}{\partial \lambda_1})^T = f_1(x_1,x_2) + B_1(x_1,x_2)u, \quad x_1(t_0), \tag{4a}$$

$$\varepsilon\dot{x}_2 = (\frac{\partial H}{\partial \lambda_2})^T = f_2(x_1,x_2) + B_2(x_1,x_2)u, \quad x_2(t_0), \tag{4b}$$

$$\dot{\lambda}_1 = -\left(\frac{\partial H}{\partial x_1}\right)^T = -\left(\frac{\partial k(x)}{\partial x_1}\right)^T k(x) - \left(\left(\frac{\partial f(x)}{\partial x_1}\right)^T + u^T\left(\frac{\partial B(x)}{\partial x_1}\right)^T + \frac{1}{2}u^T\frac{\partial R(x)}{\partial x_1}\right)\lambda \tag{4c}$$

$$, \lambda_1(x(t_F)) = \frac{1}{2}\left(\frac{\partial h}{\partial x_1}\right)^T |_{t_F},$$

$$\varepsilon\dot{\lambda}_2 = -\left(\frac{\partial H}{\partial x_2}\right)^T = -\left(\frac{\partial k(x)}{\partial x_2}\right)^T k(x) - \left(\left(\frac{\partial f(x)}{\partial x_2}\right)^T + u^T\left(\frac{\partial B(x)}{\partial x_2}\right)^T + \frac{1}{2}u^T\frac{\partial R(x)}{\partial x_2}\right)\lambda \tag{4d}$$

$$, \varepsilon\lambda_2(x(t_F)) = \frac{1}{2}\left(\frac{\partial h}{\partial x_2}\right)^T |_{t_F},$$

$$0 = \frac{\partial H}{\partial u} = R(x)u + B_1^T(x_1,x_2)\lambda_1 + B_2^T(x_1,x_2)\lambda_2. \tag{4e}$$

3.1 Description of The System As SDCs (The first step)
A continuous nonlinear matrix-valued function $A(x)$ always exists such that
$f(x)=A(x)x$ (5)

Where $A(x):R^n\rightarrow R^{n\times n}$ is found by mathematical factorization and is, clearly, non-unique when $n>1$. A suitable choice for matrix $A(x)$ is $A(x) = \int_0^1 \frac{\partial f}{\partial x}|_{x=\alpha x} d\alpha$, where α is a dummy variable that was introduced in the integration [1]. Then, the relations (4) can be written as:

$$E\dot{x} = A(x)x + B(x)u, \quad x(t_0) \tag{6a}$$

$$E\dot{\lambda} = -(\frac{\partial H}{\partial x})^T = -\left(\frac{\partial k(x)}{\partial x}\right)^T k(x) - \left(\left(\frac{\partial f(x)}{\partial x}\right)^T + u^T\left(\frac{\partial B(x)}{\partial x}\right)^T + \frac{1}{2}u^T\frac{\partial R(x)}{\partial x}\right)\lambda, \; E\lambda(x(t_f)) = \frac{1}{2}\left(\frac{\partial h}{\partial x}\right)^T|_{t_f} \tag{6b}$$

$$u = -R^{-1}(x)B^T(x)\lambda \tag{6c}$$

Considering that *B(x)* and *R(x)* are nonzero, the optimal control law is proportional to vector λ.

3.2 Description of The Hamiltonian Matrix As SDCs (The second step)

Assuming that $K(x) = \int_0^1 \frac{\partial k}{\partial x}|_{x=\alpha x} d\alpha$ is available from *k(x)=K(x)x* and that *Q(x)=K^T(x)K(x)* and *S(x)=B(x)R^{-1}(x)B^T(x)*, the relations (6) can be rewritten as follow:

$$E\dot{x} = A(x)x - S(x)\lambda, \quad x(t_0) = x_0, \tag{7a}$$

$$E\dot{\lambda} = -Q(x)x - A^T(x)\lambda - [\sum_{i=1}^{n} x_i\left(\frac{\partial K_i(x)}{\partial x}\right)^T k(x)$$

$$+ \{\sum_{i=1}^{n} x_i\left(\frac{\partial A_i(x)}{\partial x}\right)^T + \frac{1}{2}\sum_{i=1}^{m}\left(\left(\lambda^T B(x)R^{-1}(x)\right)_i \frac{\partial R_i(x)}{\partial x}\right)R(x)^{-1}B^T(x) - \sum_{i=1}^{m}\left(\lambda^T B(x)R^{-1}(x)\right)_i\left(\frac{\partial B_i(x)}{\partial x}\right)^T\}\lambda], \tag{7b}$$

$$E\lambda(x(t_F)) = \frac{1}{2}\left(\frac{\partial h}{\partial x}\right)^T|_{t_F},$$

Where,

$$\frac{\partial A_i(x)}{\partial x} = \begin{bmatrix} \frac{\partial A_{1i}(x)}{\partial x_1} & \cdots & \frac{\partial A_{1i}(x)}{\partial x_n} \\ \vdots & \ddots & \vdots \\ \frac{\partial A_{ni}(x)}{\partial x_1} & \cdots & \frac{\partial A_{ni}(x)}{\partial x_n} \end{bmatrix}, \tag{8a}$$

$$\frac{\partial K_i(x)}{\partial x} = \begin{bmatrix} \frac{\partial K_{1i}(x)}{\partial x_1} & \cdots & \frac{\partial K_{1i}(x)}{\partial x_n} \\ \vdots & \ddots & \vdots \\ \frac{\partial K_{ni}(x)}{\partial x_1} & \cdots & \frac{\partial K_{ni}(x)}{\partial x_n} \end{bmatrix}, \tag{8b}$$

$$\frac{\partial B_i(x)}{\partial x} = \begin{bmatrix} \frac{\partial B_{1i}(x)}{\partial x_1} & \cdots & \frac{\partial B_{1i}(x)}{\partial x_n} \\ \vdots & \ddots & \vdots \\ \frac{\partial B_{ni}(x)}{\partial x_1} & \cdots & \frac{\partial B_{ni}(x)}{\partial x_n} \end{bmatrix}, \tag{8c}$$

$$\frac{\partial R_i(x)}{\partial x} = \begin{bmatrix} \dfrac{\partial R_{1i}(x)}{\partial x_1} & \cdots & \dfrac{\partial R_{1i}(x)}{\partial x_n} \\ \vdots & \ddots & \vdots \\ \dfrac{\partial R_{mi}(x)}{\partial x_1} & \cdots & \dfrac{\partial R_{mi}(x)}{\partial x_n} \end{bmatrix}. \tag{8d}$$

Assumption 1: $A(x)$, $B(x)$, $Q(x)$, $R(x)$, $\dfrac{\partial A(x)}{\partial x}, \dfrac{\partial B(x)}{\partial x}, \dfrac{\partial K(x)}{\partial x}$ and $\dfrac{\partial R(x)}{\partial x}$ are bounded in a

neighborhood of Ω about the region. Then, the expression in the bracket will be ignored because of being small. This approximation is asymptotically optimal, in that it converges to the optimal control close to the origin as [2]. Thus, the relations (7) can be written as:

$$\begin{bmatrix} E\dot{x} \\ E\dot{\lambda} \end{bmatrix} = \begin{bmatrix} A(x) & -S(x) \\ -Q(x) & -A^T(x) \end{bmatrix} \begin{bmatrix} x \\ \lambda \end{bmatrix} \tag{9}$$

Remark 1: Suppose that T_{si}, T_{sF} are dominant time constants of the slow subsystem for initial and

final layer correction, respectively. In other words, $T_{si} = \max \dfrac{1}{\left| real\left(eig_{slow}(J_i)\right)\right|}$ and

$T_{sF} = \max \dfrac{1}{\left| real\left(eig_{slow}(J_F)\right)\right|}$ where, J_i and J_F are the Jacobian matrices of Hamiltonian system in

initial and final layer correction and, $J_i \cong \begin{bmatrix} A(x) & -S(x) \\ -Q(x) & -A^T(x) \end{bmatrix}_{\substack{t=t_0 \\ x=x_0 \\ \lambda \to 0_n}}, J_F \cong \begin{bmatrix} A(x) & -S(x) \\ -Q(x) & -A^T(x) \end{bmatrix}_{\substack{t=t_F \\ x \to 0_n \\ \lambda \to 0_n}}$.

Note that $(T_{si}+T_{sF})/2$ is the average time constant of the Hamiltonian system and the setting time is fourfold of one, then a proper selection for t_F is

$$t_F > t_0 + 2(T_{si} + T_{sF}) \tag{10}$$

3.3 The Singularly Perturbed SDRE in Finite Horizon

In the proposed method, co-sate vector λ, can be described as $\lambda = P(x)x$ using the sweep method

[3], where, $P(x) = \begin{bmatrix} P_{11}(x_1, x_2) & \varepsilon P_{21}^T(x_1, x_2) \\ P_{21}(x_1, x_2) & P_{22}(x_1, x_2) \end{bmatrix}, P_{ij} \in R^{n_i \times n_j}$ [7] is the unique, non-symmetric,

positive-definite solution of the Riccati matrix equation. By differentiating λ with respect to time, we can write:

$$\dot{\lambda} = P(x)\dot{x} + \dot{P}(x)x \tag{11}$$

By substituting (11) in (9) and with rearrangement of one, we have:

$$E\dot{P}(x) + P^T(x)A(x) + A^T(x)P(x) - P^T(x)S(x)P(x) + Q(x) = 0_{n \times n}, P(x(t_F)) = \frac{E^{-1}}{2}\int_0^1 \frac{\partial}{\partial x}\left(\frac{\partial h}{\partial x}\right)^T \Big|_{x=\alpha x} d\alpha \tag{12}$$

The relation (12) is called a SDRE for nonlinear singularly perturbed system in finite horizon. It should be noted that the optimal control law is obtained by computing these Riccati matrices.

The solution conditions for SDRE are that $\{A(x),B(x)\}$ be stabilizable and $\{A(x),(Q(x))^{1/2}\}$ be detectable for $\forall x \in R^n$. A sufficient test for the stabilizability condition of $\{A(x),B(x)\}$ is to check that the controllability matrix $M_c = [B(x),A(x)B(x),\ldots,A^{n-1}(x)B(x)]$ has rank$(M_c)=n$, $\forall x \in \Omega$. Similarly, a sufficient test for detectability of $\{A(x), (Q(x))^{1/2}\}$ is that the observability matrix $M_o = [(Q(x))^{1/2}, (Q(x))^{1/2}A(x),\ldots, (Q(x))^{1/2}A^{n-1}(x)]$ has rank$(M_o)=n$, $\forall x \in \Omega$ [2]. Furthermore, the closed-loop matrix $A(x)-S(x)P(x)$ should be pointwise Hurwitz for $\forall x \in \Omega$. Here, Ω is any region such that the

Lyapunov function $V(x) = x^T\left(\int_0^1 \alpha P(\alpha x)d\alpha\right)x$ is locally Lipschitz around the origin [2]. The SDRE in

(12) consist $\dfrac{(n_1 + n_2)(n_1 + n_2 + 1)}{2}$ differential equations that number of these equations is reduced by using singular perturbation theory.

3.4   The Separated Hamiltonian Matrices

In the proposed method, by separating the slow and fast variables as $X_s = \begin{bmatrix} x_1 \\ \lambda_1(x_1, x_2) \end{bmatrix}$,

$X_f = \begin{bmatrix} x_2 \\ \lambda_2(x_1, x_2) \end{bmatrix}$, we can describe the optimization relations (9) in the form of the following

singularly perturbed state-dependent Hamiltonian matrix:

$$\begin{bmatrix} \dot{X}_s \\ \varepsilon \dot{X}_f \end{bmatrix} = \begin{bmatrix} H_{11}(x_1, x_2) & H_{12}(x_1, x_2) \\ H_{21}(x_1, x_2) & H_{22}(x_1, x_2) \end{bmatrix} \begin{bmatrix} X_s \\ X_f \end{bmatrix}, \tag{13}$$

Where, $H_{ij}(x_1, x_2) = \begin{bmatrix} A_{ij}(x_1, x_2) & -S_{ij}(x_1, x_2) \\ -Q_{ij}(x_1, x_2) & -\left(A_{ji}(x_1, x_2)\right)^T \end{bmatrix}$ and $I, j = 1,2$. Thus, we assume that the $2n_1$

eigenvalues of the system (13) are pointwise small and the remaining $2n_2$ eigenvalues are pointwise large, corresponding to the slow and fast responses, respectively. The state and co-state equations (13) constitute a singularly perturbed, two point boundary value problem (TPBVP). Hence, the asymptotic solution is obtained as an *outer* solution in terms of the original

independent variable t, *initial* layer correction in terms of an initial stretched variable $\tau = \dfrac{t - t_0}{\varepsilon}$,

and *final* layer correction in terms of a final stretched variable $\sigma = \dfrac{t_F - t}{\varepsilon}$ [5]. Thus, the

composite solutions can be written as follow:

$$\begin{cases} x_1(t, \varepsilon) = x_{1o}(t, \varepsilon) + x_{1i}(\tau, \varepsilon) + x_{1F}(\sigma, \varepsilon) \\ x_2(t, \varepsilon) = x_{2o}(t, \varepsilon) + x_{2i}(\tau, \varepsilon) + x_{2F}(\sigma, \varepsilon) \\ P_s(t, \varepsilon) = P_{so}(t, \varepsilon) + P_{si}(\tau, \varepsilon) + P_{sF}(\sigma, \varepsilon) \\ P_f(t, \varepsilon) = P_{fo}(t, \varepsilon) + P_{fi}(\tau, \varepsilon) + P_{fF}(\sigma, \varepsilon) \end{cases} \tag{14}$$

where $t_0 \le t \le t_F, 0 \le \tau \le t_1 \prec \dfrac{t_F - t_0}{\varepsilon}, 0 \le \sigma \le t_2 \prec \dfrac{t_F - t_0}{\varepsilon}$. The first terms on the right hand sides of

the above relations represent the outer solution. The second and third terms represent boundary-layer corrections to the slow manifold near the initial and final times, respectively. Indices *o, i* and *F* correspond to the outer layer, initial, and final correction layers. For any boundary condition on the slow manifold, states and co-states are given by outer solution. For any boundary condition out of the slow manifold, the trajectory rapidly approaches the slow manifold according to the fast manifolds.

We now perform the slow-fast decomposition of the singularly perturbed state-dependent Hamiltonian matrix, in which $H_{22}(x_1, x_2)$ must be non-singular for all x_1, x_2 (in what follows, dependence upon x_1, x_2 is not represented, for convenience):

$$\begin{bmatrix} H_{11} & H_{12} \\ \dfrac{H_{21}}{\varepsilon} & \dfrac{H_{22}}{\varepsilon} \end{bmatrix} = \begin{bmatrix} I_{2n_1 \times 2n_1} & \varepsilon H_{12} H_{22}^{-1} \\ -0_{2n_2 \times 2n_2} & I_{2n_2 \times 2n_2} \end{bmatrix} \times$$

$$\begin{bmatrix} H_{11} - H_{12} H_{22}^{-1} H_{21} & 0_{2n_1 \times 2n_2} \\ 0_{2n_2 \times 2n_1} & \dfrac{H_{22}}{\varepsilon} \end{bmatrix} \times \begin{bmatrix} I_{2n_1 \times 2n_1} & 0_{2n_1 \times 2n_2} \\ H_{22}^{-1} H_{21} & I_{2n_2 \times 2n_2} \end{bmatrix} \tag{15}$$

Stated differently:

$$
\begin{bmatrix} I_{2n_1 \times 2n_1} & -\varepsilon H_{12}H_{22}^{-1} \\ 0_{2n_2 \times 2n_1} & I_{2n_2 \times 2n_2} \end{bmatrix} \begin{bmatrix} \dot{X}_s \\ \dot{X}_f \end{bmatrix} = \begin{bmatrix} H_{11} - H_{12}H_{22}^{-1}H_{21} & 0_{2n_1 \times 2n_2} \\ 0_{2n_2 \times 2n_1} & \dfrac{H_{22}}{\varepsilon} \end{bmatrix}
$$
$$
\times \begin{bmatrix} I_{2n_1 \times 2n_1} & 0_{2n_1 \times 2n_2} \\ H_{22}^{-1}H_{21} & I_{2n_2 \times 2n_2} \end{bmatrix} \begin{bmatrix} X_s \\ X_f \end{bmatrix}
$$

(16)

New co-sate vector can be described as $\lambda_{new} = P_{new}(x_{new})x_{new}$, where $x_{new} = \begin{bmatrix} x_s \\ x_f \end{bmatrix}$,

$\lambda_{new} = \begin{bmatrix} \lambda_s(x_s, x_f) \\ \lambda_f(x_s, x_f) \end{bmatrix}$, $\lambda_s \in R^{n_1}, \lambda_f \in R^{n_2}$, and $P_{new}(x_{new}) = \begin{bmatrix} P_s(x_s, x_f) & \varepsilon P_a(x_s, x_f) \\ \varepsilon P_b(x_s, x_f) & P_f(x_s, x_f) \end{bmatrix}$. Then, the

new slow-fast variables are defined as follow:

$$
\chi_s = \begin{bmatrix} x_s \\ \lambda_s(x_s, x_f) \end{bmatrix} = X_s,
$$

(17a)

$$
\chi_f = \begin{bmatrix} x_f \\ \lambda_f(x_s, x_f) \end{bmatrix} = H_{22}^{-1}H_{21}X_s + X_f,
$$

(17b)

Thus, (13) is converted to a new form:

$$
\begin{cases} \dot{X}_s - \varepsilon H_{12}H_{22}^{-1}\dot{X}_f = \left(H_{11} - H_{12}H_{22}^{-1}H_{21}\right)\chi_s \\ \varepsilon \dot{X}_f = H_{22}\chi_f \end{cases}
$$

(18)

Finally, the optimization equations in a singular perturbation model framework with the new variables are obtained as:

$$
\begin{cases} \dot{\chi}_s = \left(H_{11} - H_{12}H_{22}^{-1}H_{21}\right)\chi_s + H_{12}\chi_f \\ \varepsilon \dot{\chi}_f = \varepsilon H_{22}^{-1}H_{21}\left(H_{11} - H_{12}H_{22}^{-1}H_{21}\right)\chi_s + \varepsilon\left(-H_{22}^{-1}\dot{H}_{22}H_{22}^{-1}H_{21} + H_{22}^{-1}\dot{H}_{21}\right)\chi_s + \left(H_{22} + \varepsilon H_{22}^{-1}H_{21}H_{12}\right)\chi_f \end{cases}
$$

(19)

Moreover, the separated state-dependent Hamiltonian matrices $H_s(x_s, x_f)$ and $H_{22}(x_1, x_2)$ are described in the form of the following:

$$
H_s(x_s, x_f) = H_{11}(x_1, x_2) - H_{12}(x_1, x_2)H_{22}^{-1}(x_1, x_2)H_{21}(x_1, x_2) + [O(\varepsilon)]_{2n_1 \times 2n_1}
$$
$$
= \begin{bmatrix} A_s(x_1, x_2)_{n_1 \times n_1} & -S_s(x_1, x_2)_{n_1 \times n_1} \\ -Q_s(x_1, x_2)_{n_1 \times n_1} & -\left(A_s(x_1, x_2)\right)^T_{n_1 \times n_1} \end{bmatrix} + [O(\varepsilon)]_{2n_1 \times 2n_1},
$$

(20a)

$$
H_f(x_s, x_f) = H_{22}(x_1, x_2) + [O(\varepsilon)]_{2n_2 \times 2n_2} = \begin{bmatrix} A_{22}(x_1, x_2)_{n_2 \times n_2} & -S_{22}(x_1, x_2)_{n_2 \times n_2} \\ -Q_{22}(x_1, x_2)_{n_2 \times n_2} & -\left(A_{22}(x_1, x_2)\right)^T_{n_2 \times n_2} \end{bmatrix} + [O(\varepsilon)]_{2n_2 \times 2n_2}.
$$

(20b)

3.5 The slow-fast SDREs (The third step)

In the proposed method, using the singular perturbation theory, the subsystems (19) are converted into outer-layer and boundary-layer correction subsystems. The separated SDRE relations are, then derived and solved for obtaining the optimal control law.

Theorem 1: The singularly perturbed system (1) with performance index (2) is assumed. The slow- fast state equations in the initial layer correction are obtained as follow:

$$\dot{x}_{1o} = \left(A_s(x_{1o}, x^*_{2o} + x_{2i}) - S_s(x_{1o}, x^*_{2o} + x_{2i})P_{so}\right)x_{1o}, x_{1o}|_{t_0} = x_1(t_0), \tag{21a}$$

$$\frac{dx_{2i}}{d\tau} = \left(A_{22}(x_{1o}, x^*_{2o} + x_{2i}) - S_{22}(x_{1o}, x^*_{2o} + x_{2i})P^*_{22o}\right)\left(x^*_{2o} + x_{2i}\right) +$$

$$\left(A_{21}(x_{1o}, x^*_{2o} + x_{2i}) - S_{21}(x_{1o}, x^*_{2o} + x_{2i})P_{so} - S_{22}(x_{1o}, x^*_{2o} + x_{2i})P^*_{21o}\right)x_{1o}, x_{2i}|_{t_0} = x_2(t_0) - x^*_{2o}(t_0), \tag{21b}$$

Also, the slow- fast SDREs in the final layer correction are obtained as follow:

$$\dot{P}_{so} + P_{so}A_{so}(x_{1o}, x^*_{2o}) + A_{so}^T(x_{1o}, x^*_{2o})P_{so} - P_{so}S_{so}(x_{1o}, x^*_{2o})P_{so} +$$

$$Q_{so}(x_{1o}, x^*_{2o}) = 0_{n_1 \times n_1}, P_{so}|_{t_F} = P_{11}(t_F), \tag{22a}$$

$$\frac{dP_{fF}}{d\sigma} = P_{fF}\left(A_{22o} - S_{22o}P^*_{22o}\right) + \left(A_{22o}^T - P^*_{22o}S_{22o}\right)P_{fF} - P_{fF}S_{22o}P_{fF}, P_{fF}|_{t_F} = P_{22}(t_F) - P^*_{22o}(t_F). \tag{22b}$$

where, $\begin{bmatrix} P_{11}(x(t_F)) & \varepsilon P_{21}^T(x(t_F)) \\ P_{21}(x(t_F)) & P_{22}(x(t_F)) \end{bmatrix} = \frac{E^{-1}}{2}\int_0^1 \frac{\partial}{\partial x}\left(\frac{\partial h}{\partial x}\right)^T|_{x=\alpha x} d\alpha$. Furthermore, the optimal control law is as follows:

$$u = -R^{-1}(x_{1o}, x^*_{2o} + x_{2i})\left(B_1^T(x_{1o}, x^*_{2o} + x_{2i})P_{so}x_{1o} + B_2^T(x_{1o}, x^*_{2o} + x_{2i})\left(P_c x_{1o} + \left(P^*_{22o} + P_{fF}\right)\left(x^*_{2o} + x_{2i}\right)\right)\right) \tag{23}$$

where, P_{so} and P_{fF} are the unique, symmetric, positive-definite solutions of (22), and

$$P_c = \left[P^*_{22o} + P_{fF} \quad -I_{n_2 \times n_2}\right]H_{22}^{-1}(x_{1o}, x^*_{2o} + x_{2i})H_{21}(x_{1o}, x^*_{2o} + x_{2i})\begin{bmatrix} I_{n_1 \times n_1} \\ P_{so} \end{bmatrix}.$$ The solution necessary conditions of relations (21) and (22) are as follow:

- $\{A_{so}(x_{1o}, x^*_{2o}), B_{so}(x_{1o}, x^*_{2o})\}$ and $\{A_{22o}(x_{1o}, x^*_{2o}), B_{2o}(x_{1o}, x^*_{2o})\}$ should be stabilizable for $\forall (x_{1o}, x^*_{2o}) \in R^{n_1} \times R^{n_2}$.
- $\{A_{so}(x_{1o}, x^*_{2o}), (Q_{so}(x_{1o}, x^*_{2o}))^{1/2}\}$ and $\{A_{22o}(x_{1o}, x^*_{2o}), (Q_{22o}(x_{1o}, x^*_{2o}))^{1/2}\}$ should be detectable for $\forall (x_{1o}, x^*_{2o}) \in R^{n_1} \times R^{n_2}$.
- The outer equations (24) should have solutions (the slow manifolds) as $x^*_{2o}(x_{1o}, P_{11o})$, $P^*_{21o}(x_{1o}, P_{11o})$ and $P^*_{22o}(x_{1o}, P_{11o})$

$$\left(A_{21o} - S_{21o}P_{11o} - S_{22o}P_{21o}\right)x_{1o} + \left(A_{22o} - S_{22o}P_{22o}\right)x_{2o} = 0_{n_2}, \tag{24a}$$

$$\left(A_{22o}^T - P_{22o}S_{22o}\right)P_{21o} + \left(A_{12o}^T - P_{22o}S_{21o}\right)P_{11o} + P_{22o}A_{21o} + Q_{21o} = 0_{n_1 \times n_2}, \tag{24b}$$

$$P_{22o}A_{22o} + A_{22o}^T P_{22o} - P_{22o}S_{22o}P_{22o} + Q_{22o} = 0_{n_2 \times n_2}, \tag{24c}$$

It should be noted that in the above relations, all the elements of the state and Riccati matrices are dependent on state variables, and have not been represented for simplicity.□
Proofs of the theorems are given in appendix.
Remark 2: SDREs in (22) have $n_1 n_2$ the less differential equations respect to (12).

4. EXAMPLE

Consider a single link flexible joint robot manipulator as it has been introduced in [11]. This link is directly actuated by a D.C. electrical motor whose rotor is elastically coupled to the link. In this example, the mathematical model of system is as follows:

$$I\ddot{q}_1 + mgl\sin(q_1) + k(q_1 - q_2) = 0 \tag{25}$$

$$I\ddot{q}_2 + \beta\dot{q}_2 - k(q_1 - q_2) = u$$
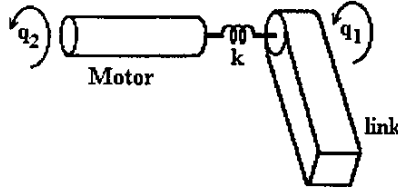
FIGURE 2: Single link flexible joint robot manipulator

In Table 1 there is a complete list of notations of the mathematical model of a single link flexible joint robot manipulator.

Notation	Description
q_1	angular positions of the link
q_2	angular positions of the motor
u	actuator force (motor torque)
I	the arm inertia
J	the motor inertia
β	the motor viscous friction
mgl	the nominal load in the rotor link
K	the stiffness coefficient of flexible joint

TABLE 1: Notations the mathematical model of a single link flexible joint robot manipulator.

Moreover, parameter values are given in Table 2.

parameter	Value of parameter
I	$0.031(Kg.m^2)$
J	$0.004(Kg.m^2)$
β	0.007
k	7.13
mgl	0.8 (N.m)

TABLE 2: Parameter values of the single link flexible joint robot manipulator.

Defining $x_1 = \begin{bmatrix} x_{11} \\ x_{12} \\ x_{13} \end{bmatrix} = \begin{bmatrix} q_1 \\ q_2 \\ \dot{q}_1 \end{bmatrix}, x_2 = \dot{q}_2, x = \begin{bmatrix} x_1 \\ x_2 \end{bmatrix}$ and $\varepsilon = J$, state equations are as follow:

$$\begin{bmatrix} \dot{x}_{11} \\ \dot{x}_{12} \\ \dot{x}_{13} \\ \varepsilon\dot{x}_2 \end{bmatrix} = \begin{bmatrix} x_{13} \\ x_2 \\ -\frac{mgl}{I}\sin(x_{11}) - \frac{k}{I}x_{11} + \frac{k}{I}x_{12} \\ kx_{11} - kx_{12} - \beta x_2 \end{bmatrix} + \begin{bmatrix} 0 \\ 0 \\ 0 \\ 1 \end{bmatrix} u, x_0 = \begin{bmatrix} 10^0 \\ 3^0 \\ 0^{0/s} \\ 0^{0/s} \end{bmatrix} \tag{26}$$

It is desired to obtain the optimal control law such that the following performance index $\mathcal{J}$ is minimized.

$$\mathcal{J} = \int_0^5 \left(x_{11}^2 + x_{12}^2 + x_{13}^2 + x_2^2 + u^2 \right) dt \tag{27}$$

In this example, $f(x) = \begin{bmatrix} x_{13} \\ x_2 \\ -\dfrac{mgl}{I}\sin(x_{11}) - \dfrac{k}{I}x_{11} + \dfrac{k}{I}x_{12} \\ kx_{11} - kx_{12} - \beta x_2 \end{bmatrix}$, $B(x) = \begin{bmatrix} 0 \\ 0 \\ 0 \\ 1 \end{bmatrix}$, $k(x) = \begin{bmatrix} x_{11} \\ x_{12} \\ x_{13} \\ x_2 \end{bmatrix}$, $R(x) = 1$, and

$h(x(t_F))=0$. Moreover, $f(x)$, $k(x)$ are differentiable with respect to x for a sufficient number of times and $x=0_4$ is the equilibrium point of the system. Furthermore, $t_0=0$, $t_F=5$, $P(x(t_F))=0_{4\times4}$.

Step 1 (Description of the system as SDCs):
To solve the optimization problem, the nonlinear functions $f(x)$, $k(x)$ must first be represented as SDCs. A suitable choice, considering [1], is as follows:

$$A(x) = \int_0^1 \frac{\partial f}{\partial x}\bigg|_{x=\alpha x} d\alpha = \begin{bmatrix} 0 & 0 & 1 & 0 \\ 0 & 0 & 0 & 1 \\ -\dfrac{mgl\sin(x_{11})}{Ix_{11}} - \dfrac{k}{I} & \dfrac{k}{I} & 0 & 0 \\ k & -k & 0 & -\beta \end{bmatrix} \tag{28a}$$

$$K(x) = \int_0^1 \frac{\partial k}{\partial x}\bigg|_{x=\alpha x} d\alpha = \begin{bmatrix} 1 & 0 & 0 & 0 \\ 0 & 1 & 0 & 0 \\ 0 & 0 & 1 & 0 \\ 0 & 0 & 0 & 1 \end{bmatrix} \tag{28b}$$

Step 2 (Description of the Hamiltonian matrix as SDCs):
The separated Hamiltonian matrices can be derived:

$$H_s(x_1,x_2) = \begin{bmatrix} 0 & 0 & 1 & 0 & 0 & 0 \\ \dfrac{\beta k}{\beta^2+1} & -\dfrac{\beta k}{\beta^2+1} & 0 & 0 & -\dfrac{1}{\beta^2+1} & 0 \\ -\dfrac{mgl\sin(x_{11})}{Ix_{11}} - \dfrac{k}{I} & \dfrac{k}{I} & 0 & 0 & 0 & 0 \\ -1-\dfrac{k^2}{\beta^2+1} & \dfrac{k^2}{\beta^2+1} & 0 & 0 & -\dfrac{\beta k}{\beta^2+1} & \dfrac{mgl\sin(x_{11})}{Ix_{11}} + \dfrac{k}{I} \\ \dfrac{k^2}{\beta^2+1} & -1-\dfrac{k^2}{\beta^2+1} & 0 & 0 & \dfrac{\beta k}{\beta^2+1} & -\dfrac{k}{I} \\ 0 & 0 & -1 & -1 & 0 & 0 \end{bmatrix} \tag{29a}$$

$$H_{22}(x_1,x_2) = \begin{bmatrix} -\beta & -1 \\ -1 & -\beta \end{bmatrix} \tag{29b}$$

Step 3.1 (the outer equations):
The relations (24) have solutions as:

$$x^*_{2o} = \frac{\beta k(x_{1\,lo} - x_{12o}) - P_{so12}x_{1\,lo} - P_{so22}x_{12o} - P_{so23}x_{13o}}{\beta^2 + 1} \tag{30a}$$

$$P^*_{21o} = \begin{bmatrix} k + \dfrac{P_{so12} - \beta k}{\sqrt{\beta^2 + 1}} \\ -k + \dfrac{P_{so22} + \beta k}{\sqrt{\beta^2 + 1}} \\ \dfrac{P_{so23}}{\sqrt{\beta^2 + 1}} \end{bmatrix} \quad (30b)$$

$$P^*_{22o} = \sqrt{\beta^2 + 1} - \beta \quad (30c)$$

Moreover, $\{A_{so}(x_{1o}, x^*_{2o}) = \begin{bmatrix} 0 & 0 & 1 \\ \dfrac{\beta k}{\beta^2 + 1} & -\dfrac{\beta k}{\beta^2 + 1} & 0 \\ -\dfrac{mgl \sin(x_{1lo})}{Ix_{1lo}} - \dfrac{k}{I} & \dfrac{k}{I} & 0 \end{bmatrix}, B_{so}(x_{1o}, x^*_{2o}) = \begin{bmatrix} 0 \\ \dfrac{1}{\sqrt{\beta^2 + 1}} \\ 0 \end{bmatrix}, \left(Q_{so}(x_{1o}, x^*_{2o})\right)^{\frac{1}{2}} =$

$$\begin{bmatrix} \dfrac{1}{2} + \dfrac{\sqrt{\beta^2 + 1 + 2k^2}}{2\sqrt{\beta^2 + 1}} & \dfrac{1}{2} - \dfrac{\sqrt{\beta^2 + 1 + 2k^2}}{2\sqrt{\beta^2 + 1}} & 0 \\ \dfrac{1}{2} - \dfrac{\sqrt{\beta^2 + 1 + 2k^2}}{2\sqrt{\beta^2 + 1}} & \dfrac{1}{2} + \dfrac{\sqrt{\beta^2 + 1 + 2k^2}}{2\sqrt{\beta^2 + 1}} & 0 \\ 0 & 0 & 1 \end{bmatrix} \}$$ is stabilizable and detectable. $\{A_{22o}(x_{1o}, x^*_{2o}) = -\beta,$

$B_{2o}(x_{1o}, x^*_{2o}) = 1, \left(Q_{22o}(x_{1o}, x^*_{2o})\right)^{\frac{1}{2}} = 1\}$ is also stabilizable and detectable.

Step 3.2 (the state equations):
According to (21), state variables relations in the initial layer correction are as follow:

$$\dot{x}_{1o} = \begin{bmatrix} x_{13o} \\ \dfrac{\beta k(x_{11o} - x_{12o}) - P_{so12}x_{11o} - P_{so22}x_{12o} - P_{so23}x_{13o}}{\beta^2 + 1} \\ -\dfrac{mgl}{I} \sin(x_{1lo}) - \dfrac{k}{I} x_{1lo} + \dfrac{k}{I} x_{12o} \end{bmatrix}, x_1(t_0) = \begin{bmatrix} 10^0 \\ 3^0 \\ 0^{0/s} \end{bmatrix} \quad (31a)$$

$$\dfrac{dx_{2i}}{d\tau} = -x_{2i}\sqrt{\beta^2 + 1}, x_{2i}(t_0) = \dfrac{7\beta k - 10P_{so12}(t_0) - 3P_{so22}(t_0)}{\beta^2 + 1}^0 \quad (31b)$$

Step 3.3 (the slow-fast SDREs):
The slow- fast SDREs in (22) have *3* the less equations respect to the original SDRE.
Considering (22), the SDRE relations in the final layer correction are as follow:

$$\dot{P}_{so} = \begin{bmatrix} \dot{P}_{s\_1lo} & \dot{P}_{s\_12o} & \dot{P}_{s\_13o} \\ \left(\dot{P}_{s\_12o}\right)^T & \dot{P}_{s\_22o} & \dot{P}_{s\_23o} \\ \left(\dot{P}_{s\_13o}\right)^T & \left(\dot{P}_{s\_23o}\right)^T & \dot{P}_{s\_33o} \end{bmatrix}, P_{so}(t_F) = 0_{3\times3}$$

$$\begin{bmatrix} \dot{P}_{s\_1lo} \\ \dot{P}_{s\_12o} \\ \dot{P}_{s\_13o} \\ \dot{P}_{s\_22o} \\ \dot{P}_{s\_23o} \\ \dot{P}_{s\_33o} \end{bmatrix} = \begin{bmatrix} \dfrac{2mglP_{so13}\sin(x_{1lo})}{Ix_{1lo}} - 1 + \dfrac{2P_{so13}k}{I} - \dfrac{2\beta kP_{so12} + k^2 - P^2_{so12}}{\beta^2 + 1} \\[2ex] \dfrac{mglP_{so23}\sin(x_{1lo})}{Ix_{1lo}} + k\dfrac{P_{so23} - P_{so13}}{I} + \beta k\dfrac{P_{sol2} - P_{so2}}{\beta^2 + 1} + \dfrac{P_{sol2}P_{so22} + k^2}{\beta^2 + 1} \\[2ex] \dfrac{mglP_{so33}\sin(x_{1lo})}{Ix_{1lo}} + \dfrac{P_{sol2}P_{so23} - \beta kP_{so23}}{\beta^2 + 1} - P_{sol1} + k\dfrac{P_{so33}}{I} \\[2ex] -2k\dfrac{P_{so23}}{I} - 1 + \dfrac{2\beta kP_{so22} - k^2 + P^2_{so22}}{\beta^2 + 1} \\[2ex] \dfrac{P_{so22}P_{so23} + \beta kP_{so23}}{\beta^2 + 1} - P_{sol2} - k\dfrac{P_{so33}}{I} \\[2ex] \dfrac{P^2_{so23}}{\beta^2 + 1} - 1 - 2P_{sol3} \end{bmatrix} \quad (32a)$$

$$\frac{dP_{fF}}{d\sigma} = -2P_{fF}\sqrt{\beta^2 + 1} + P_{fF}^2, \ P_{fF}(t_F) = -\sqrt{\beta^2 + 1} + \beta \quad (32b)$$

Step 3.4 (the optimal control law):

Moreover, the optimal control law is as follow:

$$u = \frac{k}{\beta^2 + 1}(x_{1lo} - x_{12o}) + \frac{\beta}{\beta^2 + 1}(P_{sol2}x_{1lo} + P_{so22}x_{12o} + P_{so23}x_{13o}) - (P_{fF} + \sqrt{\beta^2 + 1} - \beta)x_{2i} \quad (33)$$

The state equations and SDREs are two-point boundary value problem (TPBVP) and dependent on state variables, but we have no state values in the whole interval [0,5]. To overcome this problem we solve the above equations by an iterative procedure [3, 4]. Now, running the simulation programs, Figures 3, 4 show the angular positions and velocities.
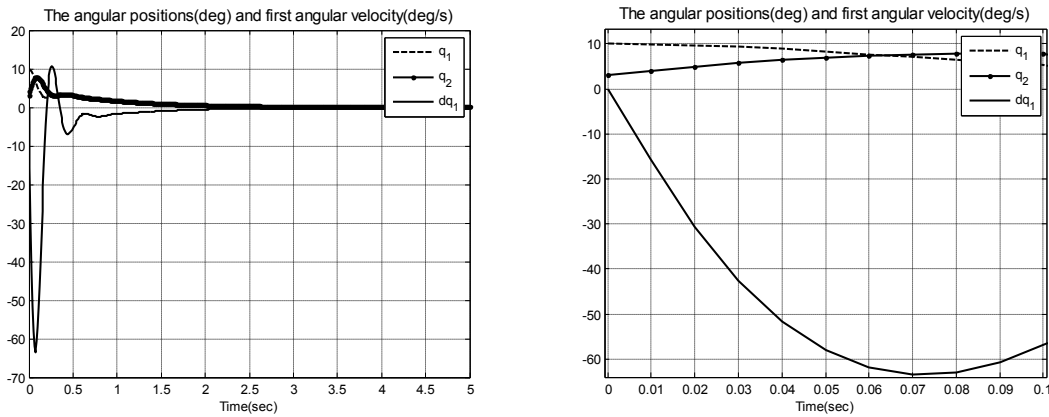
FIGURE 3: The slow state variables (The angular positions of q_1, q_2 and angular velocity of $\dot{q}_1$).
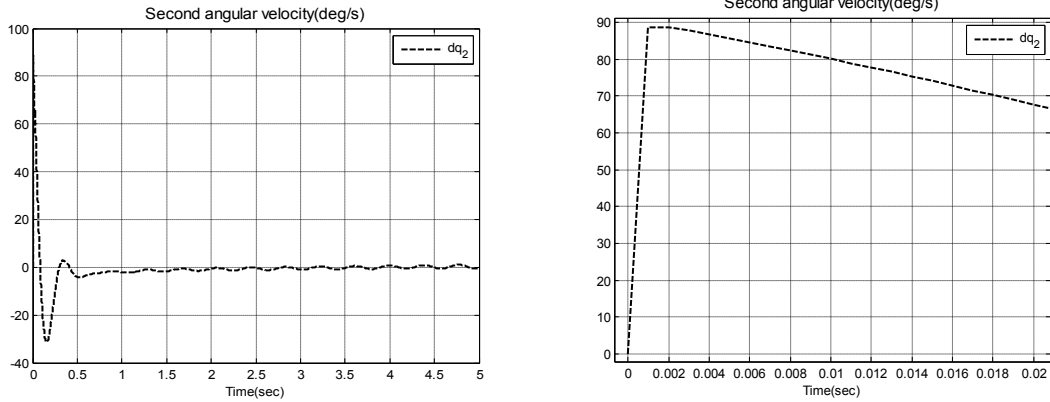
FIGURE 4: The fast state variable (angular velocity of $\dot{q}_2$).

Also, Figures 5 and 6 show the Riccati gains.
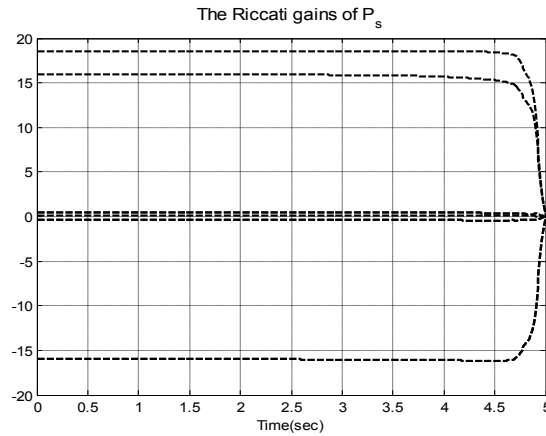
FIGURE 5: The Riccati gains of P_s.
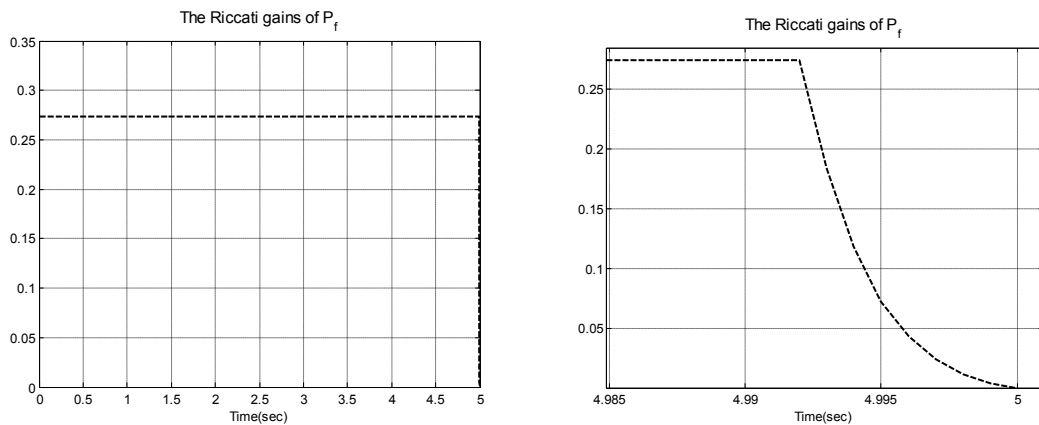
FIGURE 6: The Riccati gains of P_f.

From Figures 3 and 5, it can be seen that for any initial and final conditions on the slow manifold, for different values of ε, states are given by outer solution. On the other hand,

Figures 4 and 6 show that for any initial and final conditions out of the slow manifold, the trajectories rapidly approach the slow manifold according to the fast manifolds. Moreover, Figure 7 shows the optimal control law.
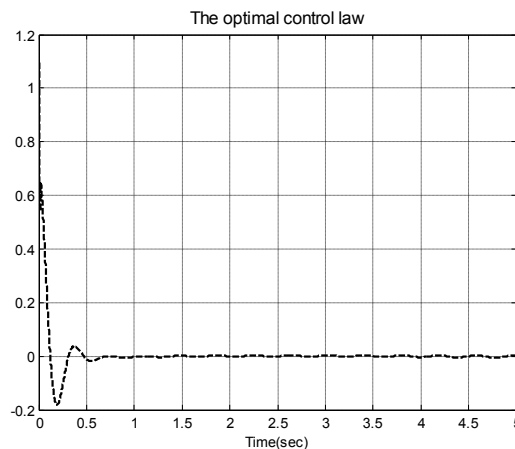
FIGURE 7: The optimal control law *u.*

5. CONCLUSION

With the proposed method in this study, it is seen that the finite-horizon optimization problem of a class of nonlinear singularly perturbed systems leads to SDREs for slow and fast state variables. One of the advantages of SDRE method is that knowledge of the Jacobian of the nonlinearity in the states, similar to HJB equation, is not necessary. Thus, the proposed method has not only simplicity of the LQ method but also higher flexibility, due to adjustable changes in the Riccati gains. On the other hand, one of the advantages of the singular perturbation theory is that it reduces high-order systems into two lower-order subsystems due to the interaction between slow and fast variables. Note that SDREs in the proposed method have $n_1 n_2$ the less differential equations respect to the original SDRE. Thus, the slow-fast SDREs have the simpler computing than original SDRE and provide good approximations of one.

6. References

[1] S.P Banks and K.J. Mhana. "Optimal Control and Stabilization for Nonlinear Systems." IMA Journal of Mathematical Control and Information, vol. 9, pp. 179-196, 1992.

[2] T. Çimen. "State-Dependent Riccati Equation (SDRE) Control: A Survey," in Proc. 17th World Congress; the International Federation of Automatic Control Seoul, Korea, 2008, pp. 3761-3775.

[3] H. Khaloozadeh and A. Abdolahi. "A New Iterative Procedure for Optimal Nonlinear Regulation Problem," in Proc. III International Conference on System Identification and Control Problems, 2004, pp. 1256-1266.

[4] H. Khaloozadeh and A. Abdolahi. "An Iterative Procedure for Optimal Nonlinear Tracking Problem," in Proc. Seventh International Conference on Control, Automation, Robotics and Vision, 2002, pp. 1508-1512.

[5] D.S. Naidu and A.J. Calise. "Singular Perturbations and Time Scales in Guidance and Control of Aerospace Systems: A Survey." Journal of Guidance, Control and Dynamics, vol. 24, no.6, pp. 1057-1078, Nov.-Dec. 2001.

[6] W.C. Su, Z. Gajic and X. Shen. "The Exact Slow-Fast Decomposition of the Algebraic Riccati Equation of Singularly Perturbed Systems." IEEE Transactions on Automatic Control, vol. 37, no. 9, pp. 1456-1459, Sep. 1992.

[7] Z. Gajic, X. Shen and M. Lim. "High Accuracy Techniques for Singularly Perturbed Control Systems-an Overview." PINSA, vol. 65, no. 2, pp. 117-127, March 1999.

[8] Z. Gajic, S. Koskie and C. Coumarbatch. "On the Singularly Perturbed Matrix Differential Riccati Equation," in Proc. CDC-ECC'05, 44th IEEE Conference on Decision and Control and European Control Conference ECC 2005, Seville, Spain,2005, pp. 14–17.

[9] R. Amjadifard and M.T. H. Beheshti. "Robust disturbance attenuation of a class of nonlinear singularly perturbed systems." International Journal of Innovative Computing, Information and Control (IJICIC), vol. 6, pp. 1349-4198, 2010.

[10] R. Amjadifard and M.T.H Beheshti. "Robust stabilization for a class of nonlinear singularly perturbed systems." Journal of Dynamic Systems, Measurement and Control (ASME), In Press, 2011.

[11] R. Amjadifard, M.J. Yazdanpanah and M.T.H. Beheshti. "Robust regulation of a class of nonlinear singularly perturbed systems," IFAC, 2005.

[12] R. Amjadifard, S.E. Khadem and H. Khaloozadeh. "Position and velocity control of a flexible Joint robot manipulator via fuzzy controller based on singular perturbation analysis," IEEE International Fuzzy Systems Conference, 2001, pp. 348-351.

[13] E. Fridman. "Exact Slow-Fast Decomposition of the Nonlinear Singularly Perturbed Optimal Control Problem." System and Control Letters, vol. 40, pp. 121-131, Jun. 2000.

[14] E. Fridman. "A Descriptor System Approach to Nonlinear Singularly Perturbed Optimal Control Problem." Automatica, vol. 37, pp. 543-549, 2001.

Appendix A: The relation between the $P(x)$ and $P_{new}(x_{new})$

In order to compute the optimal control law, the relations between the Riccati matrices

$$P(x) = \begin{bmatrix} P_{11}(x_1,x_2) & \varepsilon P_{21}{}^T(x_1,x_2) \\ P_{21}(x_1,x_2) & P_{22}(x_1,x_2) \end{bmatrix} \quad \text{and} \quad P_{new}(x_{new}) = \begin{bmatrix} P_s(x_s,x_f) & \varepsilon P_a(x_s,x_f) \\ \varepsilon P_b(x_s,x_f) & P_f(x_s,x_f) \end{bmatrix}$$ must be determined.

Suppose that $H_{22}{}^{-1}H_{21} = \begin{bmatrix} (l_{11})_{n_2 \times n_1} & (l_{12})_{n_2 \times n_1} \\ (l_{21})_{n_2 \times n_1} & (l_{22})_{n_2 \times n_1} \end{bmatrix}$, according to (17), we have:

$$\begin{cases} x_f = (l_{11} + l_{12}P_{11})x_1 + (I + \varepsilon l_{12}P_{21}{}^T)x_2, \\ p_s = P_{11} - \varepsilon(I + \varepsilon l_{12}P_{21}{}^T)^{-1}P_{21}{}^T(l_{11} + l_{12}P_{11}) + [O(\varepsilon^2)]_{n_1 \times n_1}, \\ \varepsilon p_a = \varepsilon(P_{22}l_{12} - l_{22})^{-1}P_{21}{}^T(l_{11} + l_{12}P_{11}) + [O(\varepsilon^2)]_{n_1 \times n_2}, \\ \varepsilon p_b = \varepsilon(I + \varepsilon l_{12}P_{21}{}^T)^{-1}P_{21}{}^T, \\ p_f = (P_{22} + \varepsilon l_{22}P_{21}{}^T)(I + \varepsilon l_{12}P_{21}{}^T)^{-1}, \end{cases} \tag{A1}$$

Then, for $\varepsilon = 0$, one can write:

$$\begin{bmatrix} I_{n_1 \times n_1} \\ P_s(x_s,x_f) \end{bmatrix} x_s = \begin{bmatrix} I_{n_1 \times n_1} \\ P_{11}(x_1,x_2) \end{bmatrix} x_1 \tag{A2a}$$

$$\begin{bmatrix} I_{n_2 \times n_2} \\ P_f(x_s, x_f) \end{bmatrix} x_f = H_{22}^{-1} H_{21} \begin{bmatrix} I_{n_1 \times n_1} \\ P_{11}(x_1, x_2) \end{bmatrix} x_1 + \begin{bmatrix} 0_{n_2 \times n_1} \\ P_{21}(x_1, x_2) \end{bmatrix} x_1 + \begin{bmatrix} I_{n_2 \times n_2} \\ P_{22}(x_1, x_2) \end{bmatrix} x_2 \qquad \text{(A2b)}$$

Now, multiplying (A2b) by $\begin{bmatrix} -P_f(x_s, x_f) & I_{n_2 \times n_2} \end{bmatrix}$, the following relation is obtained.

$$\left(\begin{bmatrix} -P_f(x_s, x_f) & I_{n_2 \times n_2} \end{bmatrix} H_{22}^{-1} H_{21} \begin{bmatrix} I_{n_1 \times n_1} \\ P_{11}(x_1, x_2) \end{bmatrix} + P_{21}(x_1, x_2) \right) x_1 + \left(-P_f(x_s, x_f) + P_{22}(x_1, x_2) \right) x_2 = 0_{n_2} \qquad \text{(A3)}$$

In other words, we have:

$$x_1 = x_s + [O(\varepsilon)]_{n_1} \qquad \text{(A4a)}$$

$$P_{11}(x_1, x_2) = P_s(x_s, x_f) + [O(\varepsilon)]_{n_1 \times n_1} \qquad \text{(A4b)}$$

$$P_{22}(x_1, x_2) = P_f(x_s, x_f) + [O(\varepsilon)]_{n_2 \times n_2} \qquad \text{(A4c)}$$

$$P_{21}(x_1, x_2) = P_c(x_s, x_f) + [O(\varepsilon)]_{n_2 \times n_1} \qquad \text{(A4d)}$$

Where, $P_c(x_s, x_f) = \begin{bmatrix} P_f(x_s, x_f) & -I_{n_2 \times n_2} \end{bmatrix} H_{22}^{-1} H_{21} \begin{bmatrix} I_{n_1 \times n_1} \\ P_{11}(x_1, x_2) \end{bmatrix}$. Also, for $\varepsilon=0$, we have:

$$x_{1o} = x_{so} \qquad \text{(A5a)}$$

$$P_{11o}(x_{1o}, x_{2o}) = P_{so}(x_{so}, x_{fo}) \qquad \text{(A5b)}$$

$$P_{22o}(x_{1o}, x_{2o}) = P_{fo}(x_{so}, x_{fo}) \qquad \text{(A5c)}$$

$$P_{21o}(x_{1o}, x_{2o}) = P_{co}(x_{so}, x_{fo}) \qquad \text{(A5d)}$$

Appendix B: Proof of Theorem 1

a)   The optimal control law
According to $\lambda = P(x)x$ [3] and (A4), substituting Riccati matrices in (6c), the optimal control law would result as in (23).

b)   The slow manifolds in boundary-layer correction
According to the singular perturbation theory, for $\varepsilon=0$, the fast variable should be derived with respect to the slow variable. Substituting $\varepsilon=0$ in (19), the outer-layer equations are obtained as follows:

$$\dot{\chi}_{so} = H_{s \mid \varepsilon=0} \chi_{so} + H_{12o} \chi_{fo}, \qquad \text{(B1a)}$$

$$0_{2n_2} = H_{22o} \chi_{fo}. \qquad \text{(B1b)}$$

Substituting (17b) in (B1b), the following relation is derived:

$$H_{21o} X_{so} + H_{22o} X_{fo} = 0_{2n_2}. \qquad \text{(B2)}$$

In other words, considering (14), we have:

$$(A_{21o} - S_{21o}P_{11o} - S_{22o}P_{21o})x_{1o} + (A_{22o} - S_{22o}P_{22o})x_{2o} = 0_{n_2}, \qquad \text{(B3a)}$$

$$(A_{22o}{}^T - P_{22o}S_{22o})P_{21o} + (A_{12o}{}^T - P_{22o}S_{21o})P_{11o} + P_{22o}A_{21o} + Q_{21o} = 0_{n_1 \times n_2}, \qquad \text{(B3b)}$$

$$P_{22o}A_{22o} + A_{22o}{}^T P_{22o} - P_{22o}S_{22o}P_{22o} + Q_{22o} = 0_{n_2 \times n_2}, \tag{B3c}$$

For which, $x^*_{2o}(x_{1o},P_{11o})$, $P^*_{21o}(x_{1o},P_{11o})$ and $P^*_{22o}(x_{1o},P_{11o})$ are the solutions. The necessary conditions for (B3) to be solvable, $\{A_{22o}(x_{1o},x^*_{2o}), B_{2o}(x_{1o},x^*_{2o}), (Q_{22o}(x_{1o},x^*_{2o}))^{1/2}\}$ should be pointwise stabilizable and detectable for $\forall \left(x_{1o}, x^*_{2o}\right) \in R^{n_1} \times R^{n_2}$ [2].

In (B1a), $H_{s\ |\varepsilon=0}$ for inside and out of the fast manifold, is separated as follows:

$$H_{s\ |\varepsilon=0} = H_{11}(x_1,x_2) - H_{12}(x_1,x_2)H_{22}{}^{-1}(x_1,x_2)H_{21}(x_1,x_2)_{|\varepsilon=0} =$$

$$\begin{bmatrix} A_s(x_{1o},x_2) & -S_s(x_{1o},x_2) \\ -Q_s(x_{1o},x_2) & -(A_s(x_{1o},x_2))^T \end{bmatrix}, \quad t_0 \le t \le t_0 + \varepsilon t_1, \tag{B4a}$$

$$\begin{bmatrix} A_{so}(x_{1o},x^*_{2o}) & -S_{so}(x_{1o},x^*_{2o}) \\ -Q_{so}(x_{1o},x^*_{2o}) & -(A_{so}(x_{1o},x^*_{2o}))^T \end{bmatrix}, \quad t_0 + \varepsilon t_1 \le t \le t_F. \tag{B4b}$$

Substituting (B4) in (B1a), we have:

$$\dot{x}_{1o} = \left(A_s(x_{1o},x_2) - S_s(x_{1o},x_2)P_{so}(x_{1o},x_2)\right)x_{1o}, x_{1o}|_{t_0} = x_1(t_0), \quad t_0 \le t \le t_0 + \varepsilon t_1, \tag{B5a}$$

$$\begin{bmatrix} \dot{x}_{1o} \\ P_{so}\dot{x}_{1o} + \dot{P}_{so}x_{1o} \end{bmatrix} = \begin{bmatrix} A_{so}(x_{1o},x^*_{2o})x_{1o} - S_{so}(x_{1o},x^*_{2o})P_{so}(x_{1o},x^*_{2o})x_{1o} \\ -Q_{so}(x_{1o},x^*_{2o})x_{1o} - A_{so}{}^T(x_{1o},x^*_{2o})P_{so}(x_{1o},x^*_{2o})x_{1o} \end{bmatrix}, P_{so}|_{t_F} = P_{11}(t_F), \quad t_0 + \varepsilon t_1 \le t \le t_F. \tag{B5b}$$

Thus, assuming that $\{A_{so}(x_{1o},x^*_{2o}), B_{so}(x_{1o},x^*_{2o}), (Q_{so}(x_{1o},x^*_{2o}))^{1/2}\}$ is pointwise stabilizable-detectable for $\forall \left(x_{1o}, x^*_{2o}\right) \in R^{n_1} \times R^{n_2}$ [2], with rearrangement of (B5b), the SDRE of the slow variable is obtained as (22a).

Remark 3: Note that under assumption of above, P_{so} is unique, symmetric, positive definite solution of the SDRE (22a) that produces a locally asymptotically stable closed loop solution [2]. Thus the closed-loop matrix $A_s(x_{1o},x_2)-S_s(x_{1o},x_2)P_{so}$ is pointwise Hurwitz for $\forall (x_{1o},x_2) \in \Omega_1 \times \Omega_2$. Here, $\Omega_1 \times \Omega_2$ is any region such that the Lyapunov function is locally Lipschitz around the origin.

c) The fast manifold in initial layer correction

Since the time scale will be changed as $\tau = \dfrac{t - t_0}{\varepsilon}$ in the initial layer correction, the time derivative in this scale will be changed as $\dfrac{(.)}{d\tau} = \varepsilon \dfrac{d(.)}{dt}$ in forward time. Considering (4b), we have:

$$\frac{dx_2}{d\tau} = A_{22}(x_{1o},x_2)x_2 + A_{21}(x_{1o},x_2)x_{1o} + B_2(x_{1o},x_2)u, \quad x_2|_{t_0} = x_2(t_0) \tag{B6}$$

Substituting (23) in (B6), according to (A4) and (14), the fast state equation in initial layer is obtained as (21b).

d) The fast manifold in final layer correction

Since the time scale will be changed as $\sigma = \dfrac{t_F - t}{\varepsilon}$ in the final layer correction, the time derivative in this scale will be changed as $\dfrac{d(.)}{d\sigma} = -\varepsilon \dfrac{d(.)}{dt}$ in backward time:

$$\begin{cases} \dfrac{d\chi_s}{d\sigma} = -\varepsilon \left(H_{11} - H_{12}H_{22}{}^{-1}H_{21}\right)\chi_s - \varepsilon H_{12}\chi_f \\ \dfrac{d\chi_f}{d\sigma} = -\varepsilon H_{22}{}^{-1}H_{21}\left(H_{11} - H_{12}H_{22}{}^{-1}H_{21}\right)\chi_s - \varepsilon \left(-H_{22}{}^{-1}\dot{H}_{22}H_{22}{}^{-1}H_{21} + H_{22}{}^{-1}\dot{H}_{21}\right)\chi_s - \left(H_{22} + \varepsilon H_{22}{}^{-1}H_{21}H_{12}\right)\chi_f \end{cases} \tag{B7}$$

Substituting $\varepsilon=0$ in (B7), we have $\chi_s(\sigma)=0_{2n_1}$. Therefore, the final layer correction equation is obtained as:

$$\frac{d\chi_f}{d\sigma} = -H_{22}(x_{1o}, x^*_{2o})\chi_f, \quad \chi_f\mid_{\sigma=0} = \chi_f\left(x_1(t_F), x_2(t_F)\right). \tag{B8}$$

Now, substituting (20b) and (17b) in (B8), we have:

$$\begin{bmatrix} \dfrac{dx_f}{d\sigma} \\[2mm] P_f\dfrac{dx_f}{d\sigma} + \dfrac{dP_f}{d\sigma}x_f \end{bmatrix} = -\begin{bmatrix} A_{22}(x_{1o}, x^*_{2o})x_f - S_{22}(x_{1o}, x^*_{2o})P_f x_f \\[2mm] -Q_{22}(x_{1o}, x^*_{2o})x_f - A_{22}{}^T(x_{1o}, x^*_{2o})P_f x_f \end{bmatrix}, P_f\mid_{t_F} = P_{22}(t_F), \quad t_F - \varepsilon t_2 \leq t \leq t_F. \tag{B9}$$

Thus, assuming that $\{A_{22o}(x_{1o}, x^*_{2o}), B_{2o}(x_{1o}, x^*_{2o}), (Q_{22o}(x_{1o}, x^*_{2o}))^{1/2}\}$ is stabilizable-detectable for $\forall\left(x_{1o}, x^*_{2o}\right) \in R^{n_1} \times R^{n_2}$ [2], according to (A5) and (14), the SDRE of the fast variable is obtained as (22b).

Remark 4: Note that under assumption of above, P_f is unique, symmetric, positive definite solution of the SDRE (22b) that produces a locally asymptotically stable closed loop solution [2]. Thus, the closed-loop matrix $A_{22}(x_{1o}, x_2) - S_{22}(x_{1o}, x_2)P^*_{22o}$ is pointwise Hurwitz for $\forall (x_{1o}, x_2) \in \Omega_1 \times \Omega_2$. Here, $\Omega_1 \times \Omega_2$ is any region such that the Lyapunov function is locally Lipschitz around the origin. □

Benoit Larochelle, Geert-Jan M. Kruijff & Jurriaan van Diggelen

Usage of Autonomy Features
in USAR Human-Robot Teams

Benoit Larochelle   *benoit.larochelle@dfki.de*
Language Technology Lab
German Research Center for Artificial Intelligence (DFKI GmbH)
Saarbrücken, 66121, Germany

Geert-Jan M. Kruijff   *gj@dfki.de*
Language Technology Lab
German Research Center for Artificial Intelligence (DFKI GmbH)
Saarbrücken, 66121, Germany

Jurriaan van Diggelen   *jurriaan.vandiggelen@tno.nl*
TNO Human Factors
Netherlands Organisation for Applied Scientific Research (TNO)
Soesterberg, NL-3769 DE,The Netherlands

Abstract

This paper presents the results of a high-fidelity urban search and rescue (USAR) simulation at a firefighting training site. The NIFTi was system used, which consisted of a semi-autonomous ground robot, a remote-controlled flying robot, a multiview multimodal operator control unit (OCU), and a tactical-level system for mission planning. From a remote command post, firefighters could interact with the robots through the OCU and with a rescue team in person and via radio. They participated in 40-minute reconnaissance missions and showed that highly autonomous features are not easily accepted in the socio-technological context. In fact, the operators drove three times more manually than with any level of autonomy.The paper identifies several factors, such reliability, trust, and transparency that require improvement if end-users are to delegate control to the robots, irrespective of how capable the robots are in such missions.

Keywords:autonomy, transparency, trust, situation awareness, UGV.

1. INTRODUCTION
In NIFTi we investigate how to develop cognitive robots that work together with humans. We consider robots to be, at least to some degree, autonomous actors. If they are not, we should strictly speaking not consider them as team members, but simply as tools. Lackey et al. [1] call it a "shifting paradigm of HRI from a controller/controlled relationship to a cooperative teammate relationship." We focus on the domain of Urban Search & Rescue (USAR), and particularly where robots support humans early on in making a situational assessment of the disaster site. These missions are physically and mentally stressful, which leads to real-life problems such as misunderstandings, cognitive overload, communication drop-outs, and collisions. Autonomous navigation can thus play a key role improving mission success by lowering the operators' cognitive load and allowing them to focus on other tasks.

However, a robot's autonomous capabilities and intelligence are useless if the humans in the team do not accept the robot as a team member. Recent experiences in a simulated Mars planet (desert) [2] and in the Fukushima earth quake (S. Tadokoro, p.c.) have demonstrated that whenever operators are uncertain what to expect from the robot, or do not trust the autonomy [3], they are unlikely to delegate the control and rather revert to manual control, irrespective of what the robot is able to autonomously perform.

We have jointly developed, with firefighters from the Italian fire brigade (VVF) and the Dortmund fire brigade in Germany (FDDO), a multimodal OCU for a human-robot team with various levels of autonomy[4]. The complete operator control environment allows the operator, via the OCU, to interact with a semi-autonomous unmanned ground rover (UGV), to see the feedback from a teleoperated unmanned aerial vehicle (UAV), and also to use a tactical-level system for mission planning (TRex).

In order to test our robotic system, we recreated a high-fidelity USAR scenario for a human-robot team. While traveling through a tunnel, a truck lost its load of barrels, pallets, and other assorted building materials. This caused a multicar accident where some victims are still trapped in or around cars. Most of the rescue team was in a command post at a remote location where they could safely operate the robot. We investigated how they used the robots, especially concerning autonomous features.Figure 1 shows this end-user evaluation at the *Scuola di FormazioneOperativa* (SFO) in Montelibretti, Italy, a training ground of the VVF.

FIGURE 1: End-user evaluation: tunnel accident scenario with UGV and UAV.

Overview: Below we gather various studies on the use of autonomy and then describe our end-user evaluation. Next, we present various results about operators' activities, focusing mostly on the use of autonomy features. Finally, we discuss causes and possible improvements for the acceptance of these features.

2. BACKGROUND

As early as 2004, Burke *et al.*[5] postulated that operators need adequate awareness of the robot's state and surroundings if they are to release control and use the robot's autonomy. Their suggestions have been since demonstrated in several different contexts.

In fact, improving situation awareness has always considered as a highly important issue in USAR robotics. For example, Yanco& Drury [6] performed a study of operator performance at the AAAI Robot Rescue Competition in 2002, 2003, and 2004. The authors highlighted the importance of large video feeds and the integration of all necessary information and controls in a single window. Otherwise, operators have more difficulty integrating the robot's perspective into their mental map of the area [1], [5], [6].During the three years of competition, several robots had autonomous functionalities, but most of these features were not used as the teams preferred to manually control the robots.

The recent incidents at the Fukushima Daiichi nuclear disaster site also exemplified the lack of acceptance of autonomy, as discussed by S. Tadokoro at the 2011 AAAI Fall Symposia. With low situation awareness and difficult terrain and obstacles, the operators brought a second robot only to see the main one from an exocentric perspective. The operators also preferred to manually control the robots in such difficult situations. [7]

Finally, autonomy acceptance problems exist also in the context of asynchronous interaction. Stubbs *et al.*[2] presents an outdoor robot with various levels of autonomy to explore a simulated Mars planet (desert). The authors explain that as the robot's autonomy increases, the traditional problems of perception and situation awareness leave place to problems of transparency and trust. Their conclusion is that robots must adapt their behaviors to create more realistic conversations with users. Comparing, and ideally completing, each other's knowledge should help in achieving more common ground and transparency, which are necessary if the operators are to accept – and use – the robot's autonomy.

However, sharing knowledge to establish common ground and shared situation awareness is a daunting task. Many parameters come into play, such as the users' skill levels, their familiarity with the task and the environment, the task itself, the type and modality of the information, and the timing and frequency of the exchanges between the operator and the robot [1], [8].For example, Parasuraman*et al.*[8] discuss adaptivity in providing information to operators, as well as how to avoid pitfalls of shared initiative systems. Lackey *et al.*[1] discuss how different sources of information must be understood as a whole to create high-level situation awareness in the context of mixed-initiative soldier-robot teams. The authors also prone "sharing information back-and-forth in a fluid natural manner using combinations of communication methods." Torrey *et al.*[9] shows that when executing a robot-guided task, the robot under- or over-specifying objects to which it refers can lead not only to performance problems but also to a degradation of the social cohesion. The paper also demonstrates that this phenomenon is amplified under time pressure.

3. END-USER EVALUATION
In the NIFTi project, the requirements, design, and testing phases have all been performed jointly with firefighters (end-users) from the Italian fire brigade (VVF) and the Dortmund fire brigade in Germany (FDDO). This collaboration allowed us to create highly realistic scenarios and systems, and to test them directly with end-users.

Location and Setup
In December 2011, we recreated a tunnel car accident at the SFO training site, shown in Figure 1. The area spanned 25 meters into the tunnel by a width of 10 meters, filled with debris, pallets, barrels, crashed vehicles, and smoke. Figure 5 shows a map of the area, where each grid cell represents 1 m^2. Participants had to assess the situation with one UGV and one UAV in 30 or 40 minutes, depending on whether the autonomy features were activated. The users received 30 minutes of training with the OCU, plus 15 minutes for the autonomy features. They also performed a few navigation tests before starting the scenario [10]. Ten participants, one each morning and one each afternoon for a week, participated in the experiment out of which we analyzed six complete data sets. The other four time slots were incomplete due to technical or logistical problems.

The scenario consisted of a team of responders: in the field, aUAV pilot; in a remote command post, shown in Figure 2,a mission commander and a UGV operator (experimental subject).The front row consisted of the computers that the firefighters could access. One computer with TRex[11]was available for each one of them, an OCU connected to the UAV was placed between the two, and an OCU connected to the UGV was directly in front of the operator. This set-up allowed both the operator and the mission commander to have access the high-level features of TRex, while being able to zoom in to the local situation awareness provided by any of the robots through the OCUs.

a) Picture of the command post   b) Diagram of the command post
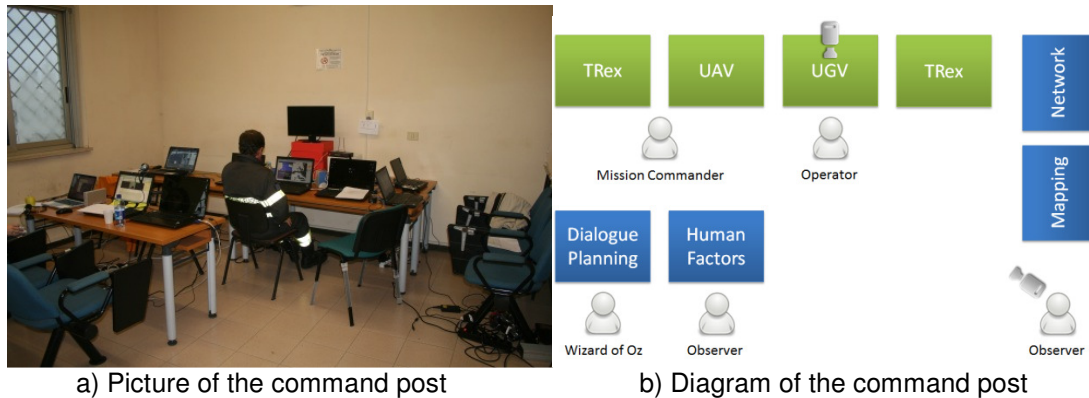
FIGURE 2: SFO December 2011: Command Post.

The other computers were used for support and debugging. One acted as a DNS/NTP server, one ran the mapping algorithms,one ran the dialogue and planning components, and finally one collected data about human factors such as heart rateand emotion through a facial recognition software. Instead of an automaticspeech recognizer,we opted for a Wizard of Oz approach, which eliminated problems due to noise and poor language skills in English. Two observers and two cameras were used.The first was a webcam clipped on the main OCU and thesecond was a standard video camera on a tripod, capturing abroad view of the scene.The set-up allowed also all support staffto oversee the experiment and freely work without disturbingthe participants.

The NIFTi System
The NIFTi system is composed of several components. First, the UGV consists of a man-portable robot with passively adaptable left and right tracks, each with motorized flippers at the front and back[12]. It has an omnidirectional camera and a rotating laser. A man-portable micro-copter was also developed to provide video feeds from two cameras.Because end-users are not accustomed to using robots and since they will be using the system under difficult conditions (i.e. varying cognitive load, high stress, loud environment, time pressure, etc.), interaction paradigms with these robots must be natural and intuitive. The UAV was actually maneuvered only from a trained pilot who received instructions from the mission commander. The video feed was broadcast in the command post.

The OCU [4]is multimodal because its two main modes of input are voice and touch with the laptop's built-in microphone and 15.6" dual-touch screen. In addition to displaying the robots' cameras' video feeds, a virtual scene is available, showing a map built up as the robot explores the environment.Laser points representing the obstacles in front of the robot and a 3D robot model are also shown. It is possible to overlay the virtual scene on top of a camera feed, which helps operators navigate in low or varying visibility (e.g. darkness, smoke).The OCU can display one, two, or four of these views simultaneously, as shown in Figure 3.The robot can automatically detect cars and victims and tells the operator via speech and text, in addition to placing iconsin the virtual scene.The robot can be manually navigated with the touch screen, but it also understands vocal commands, such as "Move forward", "Turn right" and "Go to the car".

Benoit Larochelle, Geert-Jan M. Kruijff & Jurriaan van Diggelen
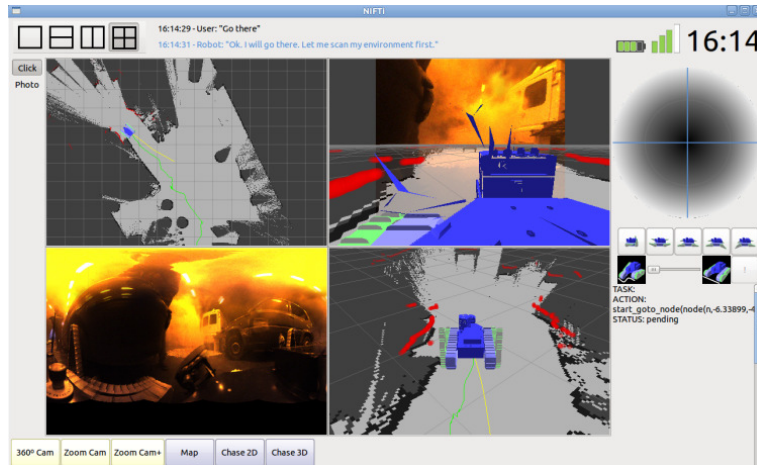
FIGURE 3: The NIFTi OCU in the tunnel accident scenario.

In addition to the OCU, we wanted to provide the rescue team with a higher-level system, hence the TRex computers. In USAR scenario, we consider that robots are operated at three levels, as detailed in [13]:

- Executional: low-level, short elementary actions (e.g. accelerating, observing objects)
- Operational: mid-level, executing a plan of actions (e.g. following a route defined during the mission)
- Tactical: high-level, planning the resources and steps (e.g. which robots will investigate which areas)

The OCU supports the executional and operational levels while the TRex system [11]supports the tactical level. The positions of the UGV and the UAV can be visualized in the TRex map, as well as localized icons representing pictures taken by the operator through the OCU and reports added by the operator and the mission commander.

4. RESULTS
We collected data for six successful missions, three with autonomy features, and three without. We are aware than this data set is quite small, but we chose to create a high-fidelity simulation with real firefighters instead of a typical lab experiment with students, even if it meant reducing the number of participants. The availability of the site and of end users made it impossible to extend the experiment to more than one week. Thus, this paper does not claim to have statistical significance like many indoors robotics experiments, but presents more data and analysis than a field report.

We synchronized the two video streams fromthe observers with recordings from all computers at the command post to prepare the results presented in this section. We expected to see clear changes in biophysical data during the missions, patterns in human-human and human-robot communication, similar driving and exploration styles among the firefighters, as well as enthusiastic use of autonomy. The results were quite different than what we expected and the salient points are presented below.

Operators' Activities

Figure 4 presents the time distribution of the six users during the scenario[1] The diagrams show that the operators spent on average 57 % of their time navigating, but with high variability. These results are very similar to last year's end-user evaluation [15] with an average of 54 % (varied from 47 % to 62 %). Burke et al [5] showed a slightly lower figure, 44%, but also with great variability. They mentioned, however, that "operators spent significantly more time gathering information about the state of the robot and the state of the environment than they did navigating" and that they "had difficulty integrating the robot's view into their understanding of the search and rescue site. They compensated for this lack of situation awareness by communicating with team members at the site". We have also experienced these problems in another field trial in July 2011 [14], but not in this end-user evaluation.
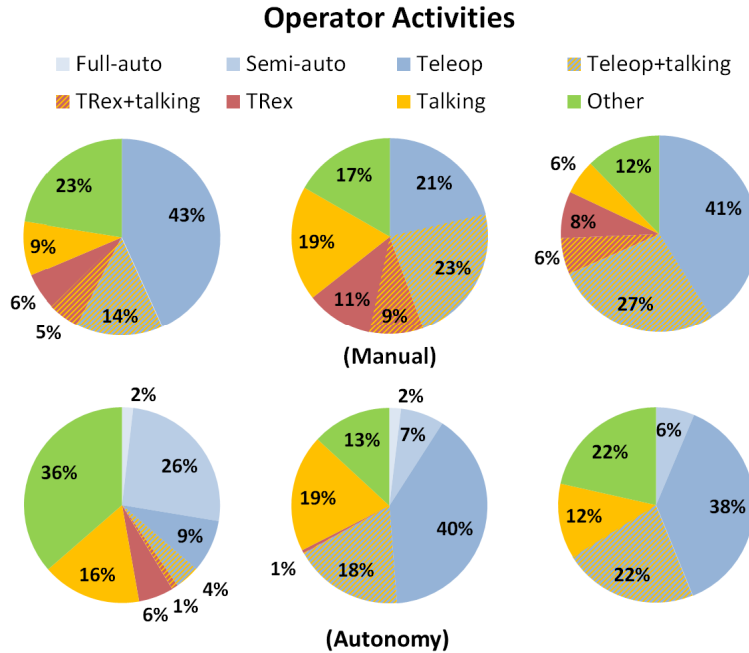
FIGURE 4: Operator activities for the six participants during the scenario.

We can also notice that the operators spent on average 35 % of their time speaking with the mission commander, again with high variability ranging from 21 % to 51 %. While talking, the operators were also navigating the robot on average 50 % of that time, with a range from 19 % to 70 %. This indicates that the operators' cognitive load was not too high to perform these two simultaneous tasks, contrary to our expectations.Finally, we notice that the operators spent on average 20 % of their time on other activities, mostly moving the camera and studying the environment through the image.

In addition to overall time distribution, we analyzed *when*did the operators do*what*. Once again, we could not identify any recurring pattern, but rather observed varied styles again. However, an interesting observation is that the users switch to a lower autonomy mode mostly after a failure of the autonomous feature. Desai *et al.*[3] also observed that users switched to lower autonomy modes quickly after the robot made mistakes, and took much longer to trust the autonomy again.Finally, the participants' heart rates were monitored but they showed nearly no variation

---

[1]Because we were not able to get a firefighter available for the whole week to play the role of the mission commander, we had one for the first three participants and another one for the last three participants. Their styles of interaction partly explain the large difference in the use of TRex.

during the scenario. They were also asked to indicate their cognitive load on a scale of 1 to 5 every two minutes, and no significant variation was observed.

Operators' Paths and Performance
Our expectations were that the operators would generally navigate around areas of interest, based on their firefighting training. However, and analysis of their paths revealed to be highly varied and we could not extract patterns in driving styles or prominent locations for stopping and observing the scenario. Figure 5a) shows the path of one of the participants, augmented with spheres that indicate how much time she spent at each location. The smallest spheres indicate 1 second while the largest indicate 15 seconds or more. Additionally, arrows with numbers indicate where the robot was at every two-minute interval.

Figure 5b) shows the same path but color-coded to indicate the level of autonomy used. The green sections show where the robot was teleoperated. The orange sections shows that the user was using semi-autonomy (short commands such as "Go forward" and "Turn left").All users started with operating the robot under autonomous mode. However, they all took back control as soon as the path became more difficult to navigate and several objects to inspect became visible. Some of the operators used autonomy features again later in the missions, but only for small movements not visible on the map. When the robot asked the users if it should autonomously go to a newly detected car, they ignored the question and continued teleoperating.

Contrary to the high variability in the paths of the six participants, their performance in finding scenario elements were quite similar. Cars were always reported, victims were found 79 % of the time, and danger signs 44 %. The results also indicate that no element was particularly hard to find and that no difference exists between the participants with and those without autonomy features.

Collisions and Situation Awareness
Teleoperation is usually considered 'bad' because it leads to frequent collisions. Our results are comparable to other studies. Table 1 shows collision data from the NIST competitions [6] and from the first NIFTi end-user evaluation [15]. Unfortunately, it is not possible to directly compare the numbers because too many variables are present. For example, scenario sizes and densities, time pressure, robot platforms, and OCUs influenced the number of collisions. In addition, we provided little user training on the NIFTi platforms but the pilots in the NIST competitions were well trained developers of the systems.

Event	NIST 2002	NIST 2003	NIST 2004	NIFTi Jan. 2011	NIFTI Jan. 2011	NIFTI Dec. 2011
Robot	Various	Various	Various	Generaal	P3-AT	NIFTi
Duration	Max 20 min.	Max 20 min.	Max 20 min.	15 min.	Max 15 min.	30, 40 min.
Collisions	6.2	2.2	1.3	3.2	1.3	9.2

TABLE 1: Collisions in the scenario.

Usage of the OCU Views
The OCU was always launched with four default views (shown in Figure 3), and all operators except one used them without any modification. In fact,some of the operators did not even use all of the views.More specifically, the 'Map' view, which shows an overallpicture of the scenario,was not used by all operators. Moreover, the mission commanders used the map view while the operators were looking at a different part of the screen. This is an interesting behavior, since both users were given a computer with TRex, which has more high-level functionalities than the OCU, but they often converged to using a single laptop. Similarly, it was observed in the NIST competitions [6] that the screens other than the main one often get ignored. In our case, it was also easier for the participants to integrate the robot's perspective with the map view than with the TRex system.

a) Time indications   b) Autonomy indications

FIGURE 5: Path Followed by One of the Participants.

5. DISCUSSIONS

Considering the expectations that we had about the use of autonomy, we can certainly say that the results are disappointing. Figure 4 and Figure 5b) clearly show how little autonomy features were used. More precisely, the operators drove three times more manually than in all autonomous modes combined. Despite these results, we continue to believe, based on studies such as [3], [6], that more autonomy would benefit the users; either in the number of collisions or in victim discovery performance. We thus present here problematic areas of the NIFTi system and evaluation methodology that impacted the use of autonomy.

Technical Reliability & Flexibility

The NIFTi platform was produced in 2011 and being inexperienced, we set the safety margins too high. In consequence, the robot often stayed still rather than risking navigating near objects or into unknown space. Since the goal of the mission was to explore space, the users quickly got frustrated and switched to a lower autonomy mode. Short commands (e.g. "Move forward") worked well, but did not offer the same flexibility as manual control. The operators sometimes

wanted to go at a specific place, so they did it themselves. To solve that problem, we are developing an approach to analyze a robot's surroundings to provide a functional-geometric interpretation of movement commands such as "Move forward". A correct interpretation will allow the robot to move an appropriate distance based on the environment rather than moving a fixed amount. We will run experiments to determine if such a behavior leads users to rely more on autonomy[16].Finally, the robot's autonomous modes were very slow. By comparing Figure 5a) and b), we see that the first stretch took more than four minutes, at which point the user started manually driving. Autonomy was never used late in the scenario when the time pressure was higher.

Cognitive Load
One of the goals of autonomous features being the reduction in cognitive load, the features are most useful under high load. However, our users indicated that their cognitive loads were always moderate – this corroborates with them talking while teleoperating. Questionnaires also showed that they did not consider teleoperation or the mission in general to be very difficult. They had thus little incentive to use any autonomy. In addition, Oviatt*et al.*[17] found out that users interact in a multimodal fashion mostly when the task at hand is difficult and the information to convey is complex. In our case, the operators controlled the robot – in a unimodal way – because it was easy and not hindering their other tasks. Gómez [18] also ran an experiment that points to the same conclusion. In his case, operators controlled either one, two, or three robots. Operators teleoperated the single robot 93 % of the total navigation time, compared to 48 % with two robots and 27 % with three.

Engaging Dialogue
Contrary to our expectations, the users never got engaged in a true dialogue with the robot. Since the robot was silent most of the time, except when detecting cars or responding to spoken navigation commands, the users did not feel that the robot was talking to them, but rather was giving debugging information. One problem is that the spoken information contained spatial information, which was not presented to the user. For example, when detecting cars, the robot alerted the operators, but did not show where they were located on the map. When prompted to "go to the car", the operators simply ignored the question.Comparatively, Torrey *et al.*[9] showed that when executing a robot-guided task, the robot under- or over-specifying objects to which it refers can lead not only to performance problems but also to a degradation of the social cohesion. The paper also demonstrates that this phenomenon is amplified under time pressure.

Transparency
From past experiences, we believed that reducing the needto teleoperate the robot would free up some time for the userto observe the environment or perform other tasks. However,autonomous robot behavior must be transparentto the operators;otherwise, they will not understand itand will be unlikely to relinquish control to the robot. Withouttransparency, not enough trust is built up and the robot remainslargely teleoperated by the operators. In fact, the negative impacts of low transparency on human-robot interaction have been suggestedbefore in [5] and were observed in [2]. More recently, S.Tadokoro discussed the same problems at the 2011 AAAIFall Symposia about experiences at the Fukushima accidentsite. Our end-user evaluation confirmed theseobservations.For example, we ensured that the NIFTi robot would always give feedback when it succeeded or failed a task, but it never explained why it failed. Given that the users did not know about the robot's safety margins, they were left confused about the robot's autonomous behavior and wondering what happened. In successful cases, the planned path was not displayed (due to technical reasons), which also made users nervous about letting the robot autonomously navigate. In many cases, the operators were wondering if they should stop, wait or try something again.

Trust and Expectations
Our users received training for manual control, in which they usually did not crash, as well as for autonomous control, in which the robot crashed a few times. These events could have led them to trust in their abilities more than in the robot's autonomy. Desai *et al.*[3] showed that in such

cases, users tend to use manual control. The users, unfamiliar with robots, also expected more reliability and functionality. In particular, they expected the flippers to automatically adjust, regardless of the autonomy mode. Komatsu and Yamada [19] showed that when agents' functionalities are lower than the users' expectations, users tend to stop interacting with these agents. Analogously, our operators stopped using autonomy features after having tried them and being disappointed.

6. FUTURE WORKS

While the NIFTi project continues to work on autonomy features, it also aims at improving the human-robot interaction during teleoperation. Questionnaires about the OCU showed that the operators did not complain about anythingparticularly bad in the OCU. They preferred manual drivingin certain cases, automated in others. Unfortunately, they did not identify what classes of scenarios or environments prompt manual override. In any case, we expect that more operating experience would be required to make such judgments.

The main request from the operators wasto improve the display of distances. Since all users made5 to 20 collisions in the scenario, we consider that an improvement is required.After the evaluation, we decided to superimpose concentric circles at 1, 2, and 5 meters around the robot's 3D model. With these aids, it is much easier to estimate distances to the surrounding obstacles. We have also added a telescopic arm and are working on a new virtual camera, both of which allow raising the point of view of the cameras and hence projecting better depth perception. The traveled path is also now shown by default.

The next problem is that even with these improved views,it is not guaranteed that the operators will use them more. Automatic adjustmentof the views was not implemented because wefirst wanted to collect data on how the operators used them. Given low usage results, we need to find innovative ways to adjust the views for the users. Onesuggestion is an automatic zoom, which zooms in on the robotat low speeds or when navigating close to obstacles. Thesensitivity of the control widget could also be adjusted withthese parameters. Such features are already available in carsand embedded navigation systems. In a subsequent end-user evaluation in November 2012, we ran a cognitive model during the missions in order to evaluate the cognitive load of the operators. Once we analyze the results and determine that they correlate with reality, we will investigate how to adjust the views in a non-disruptive manner.

Alternatively, we are also working on the integration of in-field pictures taken from either the UGV, the UAV, or an in-field rescuer. All of the pictures will be centrally collected and stored at the command post, and made available in the OCU and in TRex. Because these pictures will be geo-located, we will show them as icons on the maps, and the operators will be able to see the environment from different points of view, helping with navigation and situation awareness in general.

7. CONCLUSIONS

We organized an end-user evaluation and recorded data from six tunnel car accident missions. Firefighters used the NIFTi robots and OCU as part of a human-robot team. We have observed highly varied usage patterns, with respect to exploration strategies, driving styles, and use of autonomy. Users spent 57 % of their time navigating, although mostly manually. Autonomy features were not extensively used, and switch to lower autonomy modes happened mostly after autonomy failures.We identified several factors that could have led to low usage of autonomy and discussed several improvements that we are developing. In particular, transparency is needed for trust, and trust is needed for autonomy. Thus, the robot should be more communicative and transparent about its status and actions, other robots, and the environment. Statements that carry spatial information should convey this spatial part in a multimodal fashion. We would also like to spend more time on user training, allowing them to adjust their expectations and develop trust in the system. Additionally, we need more focused experiments to separate the effects of technical limitations versus those social effects onto the usage of autonomy features.

Benoit Larochelle, Geert-Jan M. Kruijff & Jurriaan van Diggelen

8. ACKNOWLEDGEMENTS

9. REFERENCES

[1] S. Lackey, D. Barber, L. Reinerman, N. I. Badler, and I. Hudson,"Defining next-generation multi-modal communication in human robotinteraction," in *Proceedings of the Human Factors and Ergonomics Society Annual Meeting*, vol. 55. SAGE, September 2011, pp. 461–464.

[2] K. Stubbs, P. Hinds, and D. Wettergreen, "Autonomy and commonground in human-robot interaction: A field study," *IEEE IntelligentSystems*, vol. 22, pp. 42–50, March 2007, special Issue on Interactingwith Autonomy.

[3] M. Desai, M. Medvedev, M. Vázquez, S. McSheehy, S. Gadea-Omelchenko, C. Bruggeman, A. Steinfeld, and H. Yanco, "Effects ofchanging reliability on trust of robot systems," in *Proceedings of theseventh annual ACM/IEEE international conference on Human-RobotInteraction*. ACM, 2012, pp. 73–80.

[4] B. Larochelle andG.J.M. Kruijff, "Multi-view operator control unit to improve situation awareness in USAR missions," in*Proceedings of the 21th IEEE International Symposium on Robot and Human Interactive Communication*. IEEE, 2012, pp. 1103–1108.

[5] J. Burke, R. Murphy, M. Coovert, and D. Riddle, "Moonlight inMiami: An ethnographic study of human-robot interaction in USAR,"*Human Computer Interaction*, vol. 19, no. (1–2), pp. 85–116, 2004.

[6] H. Yanco and J. Drury, "Rescuing interfaces: A multi-year studyof human-robot interaction at the AAAI robot rescue competition,"*Autonomous Robots*, vol. 22, no. 4, pp. 333–352, May 2007.

[7] E. Guizzo, E. Ackerman, M. Waibel, M. Taylor, andS. Bouchard, "Fukushima robot operator writes tell-all blog,"http://spectrum.ieee.org/automaton/robotics/industrial-robots/fukushima-robot-operator-diaries, Aug. 2011, contains the Englishtranslation of the Japanese blog from the anonymous author S.H.

[8] R. Parasuraman, K. Cosenzo, and E. de Visser, "Adaptive automationfor human supervision of multiple uninhabited vehicles: Effects onchange detection, situation awareness, and mental workload," *MilitaryPsychology*, vol. 21, pp. 270–297, 2009.

[9] C. Torrey, A. Powers, M. Marge, S. R. Fussell, and S. Kiesler,"Effects of adaptive robot dialogue on information exchange and socialrelations," in *Proceedings of the 2006 ACM Conference on Human-Robot Interaction*. Press, 2006, pp. 126–133.

[10] T. Mioch, N. Smets, and M. Neerincx, "Assessing human-robotperformances in complex situations by means of unit task tests," in*Proceedings of the 21th IEEE International Symposium on Robot andHuman Interactive Communication*. IEEE, 2012, pp. 621–626.

[11]   J. van Diggelen, K. van Drimmelen, A. Heuvelink, P. Kerbusch,M. Neerincx, S. van Trijp, E. Ubink, and B. van der Vecht, "Mutualempowerment in mobile soldier support," *Special Issue of the International Journal of Battlefield Technology on Human Factors and Battlefield Technologies*, 2012.

[12]   Bluebotics, "Patent, mobile robot," Patent, 2011, pCT/EP2011/060937.

[13]   J. van Diggelen, R. Looije, T. Mioch, M. A. Neerincx, and N. J. M.Smets, "A usage-centered evaluation methodology for unmannedground vehicles," in *Proceedings of The Fifth International Conferenceon Advances in Computer-Human Interactions (ACHI)*, 2012.

[14]   G.J.M. Kruijff. et al, "Experience in system design for human-robot teaming inurban search & rescue," in *Proceedings of Field and Service Robotics(FSR) 2012*, Matsushima/Sendai, Japan, 2012.

[15]   B. Larochelle, G.J.M. Kruijff, N. Smets, T. Mioch, and P. Groenewegen,"Establishing human situation awareness using a multi-modal operatorcontrol unit in an urban search & rescue human-robot team," in*Proceedings of the 20th IEEE International Symposium on Robot andHuman Interactive Communication*. IEEE, 2011.

[16]   S. Keshavdas andG.J.M. Kruijff, "Interpretation of Vague Scalar Predicates Expressing Direction."Technical Report, February 2013.

[17]   S. Oviatt, R. Coulston, and R. Lunsford, "When do we interact multimodally?Cognitive load and multimodal communication patterns," in*Proceedings of the International Conference on Multimodal Interfaces*. ACMPress, 2004, pp. 129–136.

[18]   A. V. Gómez, "Evolutionary design of human-robot interfaces forteaming humans and mobile robots in exploration missions," Ph.D.dissertation, Universidad Politécnica de Madrid, 2010.

[19]   T. Komatsu and S. Yamada, "Adaptation gap hypothesis: How differencesbetween users' expected and perceived agent functions affecttheir subjective impression," *Journal of Systemics, Cybernetics andInformatics*, vol. 9, no. 1, pp. 67–74, 2011.

Compensating Joint Configuration through Null Space Control in Composite Weighted Least Norm Solution

Avik Chatterjee   *avik@cmeri.res.in*
CSIR-CMERI
MG Avenue
Durgapur, 713209, India

S. Majumder   *sjm@cmeri.res.in*
CSIR-CMERI
MG Avenue
Durgapur, 713209, India

I. Basak   *indrajit.basak@me.nitdgp.ac.in*
Department of Mechanical Engineering NIT
MG Avenue
Durgapur,713209,India

Abstract

We have presented a methodology for compensating joint configuration by composite weighting in different sub spaces. It augments the weighted least norm solution by weighted residual of the current joint rate and preferred pose rate in null space, so that we can arrive at a solution which is able to handle both joint limits and preferred joint configuration simultaneously satisfying the primary task. The null space controller is formulated in conjunction with the work space controller to achieve the objective. The contribution of null space has been discussed in the formulation in two different situations including joint limits, workspace and near configuration singularities.

Keywords: Null Space Controller, Weighted Least Norm, Joint Limit, Singularity, Joint Configuration.

1. INTRODUCTION

A robotic manipulator in general sense or an articulated serial structure in particular is kinematically redundant when the number of operational space variables necessary to specify a given task, is less than the number of joints. Redundancy leads to infinite solutions for the joint space but offers greater flexibility and dexterity in motion as different constraint based or goal based criteria can be formulated as sub tasks in the solution. Two kinds of approaches have been reported in the literature to deal with this situation. One is set to exploit the null space of the Jacobian matrix in the homogeneous solution that infuses self motion of joints without affecting the task space. Typical method of this kind is gradient projection method (GPM) [1][2]. In GPM the anti-gradient of a quadratic cost function, is projected in the null space of the task Jacobian, which is reminiscent of the projected gradient method for constrained minimization. The other approach is weighted least norm (WLN) approach [3][4], which minimizes the weighted norm of joint rate. In both the cases the primary task is to follow the prescribed trajectory and there may be multiple secondary tasks or nested subtasks with priority fixation [5] [6].

GPM has been used in Joint Limit Avoidance (JLA), obstacle avoidance [7], visual servoing [4]. WLN which was introduced in JLA in [3], has been successfully exploited by others with single or multiple criteria and Close Loop Inverse Kinematics (CLIK)[8]. Null space based motion control [9] has been studied with configuration optimization [10], influence of un-weighted and inertia weighted pseudoinverse [11], proportional-integral-derivative (PID) controller considering passivity [12], task priority implementation based on behavioral scheme [13]. An elaborate

discussion with illustrations on various pros and cons of different approaches for operational space control with null space contributions has been reported in [14].

In practice, many subtasks are often needed for the control of manipulator. For example both the joint limits and the joint configuration became the basic requirements where human motion analysis is concerned. In many cases, local optimality of GPM may not provide good performance to all prioritized subtasks. WLN method is effective only for the joints limits but direct optimization of the weighted norm sum of all tasks may lead to the poor performance for all tasks. The ability of WLN to effectively handle joint limits and the self motion from null space, motivate us to presents a methodology of composite weighted least norm (CWLN) solution in conjunction with GPM. It is so called because the formulation tries to minimize the primary task objective of weighted norm of joint rate in range space and the weighted residual of the current joint rate $(\dot{q})$ and preferred pose rate $(\dot{q}_r)$ in null space (hence composite weighting in different sub spaces) so that we can arrive at a solution which is able to handle both joint limits and preferred joint configuration simultaneously satisfying the primary task.

This paper is organized as follows: Section II formulates the CWLN method from classical redundancy control methods. Section III discusses stability of the CWLN method and its regularized version. The case studies are illustrated in Section IV. Section V concludes the paper.

2. COMPOSITE WEIGHTED LEAST NORM

We focus on first and second order kinematics for the time variant task space defined as $x(t) \in \Re^{m \times 1}$ and joint space $q(t) \in \Re^{n \times 1}$ related by the direct kinematic non linear and transcendental vector function $k_t(q)$, whose time differentiation will define the non square analytic Jacobian matrix $J(q)$ $J_t^{ij}(q)$ $\partial k_t^j / \partial q_i \in \Re^{m \times n}$; $\forall n > m$, with its assumption of bounded higher order terms and linearization. We denote the desired task space positions, velocities, and accelerations as $x_d, \dot{x}_d \ and \ \ddot{x}_d$ respectively and reference or preferred joint configuration as q_r Dropping the subscript *t* for brevity, the classical forward kinematics differential relationships can be expressed as

$$\dot{x} = J(q)\dot{q}; \ and \ \ddot{x} = J(q)\ddot{q} + \dot{J}(q,\dot{q})\dot{q} \tag{1}$$

and inverse kinematics least norm (LN) general solution as

$$\dot{q} = \dot{q}_p + \dot{q}_h = J^\dagger \dot{x} + (I - J^\dagger J)\xi_1; \ \ddot{q} = J^\dagger(\ddot{x}_d - \dot{J}\dot{q}) + (I - J^\dagger J)\xi_2 \tag{2}$$

where $\dot{q}_p \in \Re(J)$ is particular solution, $\dot{q}_h \in \aleph(J)$ is homogeneous solution, $J^\dagger$ $J^T(JJ^T)^{-1}$ is the right pseudoinverse of the Jacobian, $\xi_1 \ and \ \xi_2 \in \Re^{n \times 1}$ are arbitrary vectors and $(I - J^\dagger J)$ is the null space projector. The Weighted Least Norm (WLN) solution formulates the problem as $min(\dot{q})[\mathrm{H}_1(\dot{q})] = min(\dot{q})$ $\dot{q}$ $^2 = min(\dot{q})[\dot{q}^T W_1 \dot{q}]$, st $(\dot{x} - J\dot{q}) = 0$, $\forall W_1 \in$ $^{n \times n}$ is the symmetric positive definite weighing matrix. To stabilize the ill posed condition of LN or WLN solution near singularities, Tikhonov like regularization has been used, which makes a trade off between tracking accuracy and the feasibility of the joint velocities, known as classical Damped Least Square (DLS) solution. The trade off parameter is the damping factor α. If the objective is specified through a configuration rate dependent performance criteria $\mathrm{H}_2(\dot{q})$, set to be the closest to some particular pose, hence forth called the reference configuration (q_r) the problem can be

reformulated as $min(\dot{q})[H_2(\dot{q})] = min(\dot{q})[(1/2)(\dot{q}-\dot{q}_r)^T W_2(\dot{q}-\dot{q}_r)];\quad s.t\ J\dot{q}=\dot{x};\quad \forall W_2 \in\ {}^{n\times n}$ .In our approach an augmented objective function has been formulated by combining configuration rate dependent performance criteria $H_2(\dot{q})$ for pose optimization and $H_1(\dot{q})$ for joint limit avoidance, subjected to the requirement of primary task space $(\dot{x}-J\dot{q})=0$, as $\forall H_3(\dot{q}) = H_1(\dot{q})+H_2(\dot{q})\ and\ \forall(W_1,W_2)\in\ {}^{n\times n}$, henceforth called as Composite Weighted Least Norm Solution (CWLNS) as,

$$min(\dot{q})H_3(\dot{q}) = min(\dot{q})[(1/2)\dot{q}^T W_1\dot{q} + (1/2)(\dot{q}-\dot{q}_r)^T W_2(\dot{q}-\dot{q}_r)];\ s.t\ J\dot{q}=\dot{x} \tag{3}$$

To solve this optimization problem with equality constraint, it should satisfy both the necessary condition $\nabla_{\dot{q}}L=0$ and sufficient condition $\nabla^2_{\dot{q}}L>0$, where the Lagrangian is $L(\dot{q},\lambda) = H_3(\dot{q})+\lambda(J\dot{q}-\dot{x})$ and we can directly evaluate $\nabla^2_{\dot{q}}L = (W_1+W_2)>0$, which is true for minimization. Putting the value of $\dot{q}$ from $\nabla_{\dot{q}}L=0$ in the expression $\nabla_\lambda L=0$, we get λ. Substituting λ back in $\dot{q}$ from $\nabla_{\dot{q}}L=0$, and $\forall J^\hbar\quad W^{-1}J^T(JW^{-1}J^T)^{-1},\quad \forall W\quad (W_1+W_2),\forall\xi_1\quad \dot{q}_r$, the general solution of CWLS reduces to [Appendix-I.A]

$$\dot{q} = J^\hbar\dot{x} + (I-J^\hbar J)W^{-1}W_2\xi_1 \tag{4}$$

It is trivial to show $(I-J^\hbar J)W^{-1}W_2$ is the null space projector of reference joint rate vector $\dot{q}_r$ and hence no impact on task space as $JJ^\hbar=I$. The optimization in the direction of the anti-gradient of scalar configuration dependent performance criteria $H_3(q)$ can also be set up by minimizing $H_3(q)$ for weighted reference configuration (q_r) as

$$H_3(q) = (1/2)(q-q_r)^T W_2(q-q_r); \Rightarrow \nabla_q H_3(q) = W_2(q-q_r) \tag{5}$$

and for a positive scalar k_H and $\forall\xi_1'\quad -k_H(W_1+W_2)^{-1}W_2\nabla_q H_3(q)$ the GPM flavor of CWLS formulation is

$$\dot{q} = J^\hbar\dot{x} + (I-J^\hbar J)W^{-1}W_2\xi_1';\quad \ddot{q} = J^\hbar(\ddot{x}_d - \dot{J}\dot{q}) + (I-J^\hbar J)\xi_2 \tag{6}$$

Using Eq.(2), the relation $\dot{J}J^\hbar = -J\dot{J}^\hbar$ and after simplification we can establish the relation between ξ_2 and ξ_1 as.

$$\xi_2 = \dot{J}^\hbar J(\dot{q}-\xi_1) + \dot{\xi}_1' \tag{7}$$

The diagonal elements (w_1^i) of W_1 has been utilized to implement JLA [2][3] with a modified sigmoid function to vary smoothly from -1 to 1. If τ is the threshold parameter for each joint, the activation limits are defined as $q_{i,max}^{th} = (q_{i,max}-\tau)$ and $q_{i,min}^{th} = (q_{i,min}+\tau)$. If $\Delta q_i^{th} = (q_{i,max}^{th} - q_{i,min}^{th})$ is the activation range of ith joint, then $w_i = 1 + \mu|h(q_i)|$, where $\mu=$ a large positive gain,

$$h(q_i)\begin{cases} -\varphi_i & \forall q_i < q_{i,min}^{th}+\bar{\varepsilon} \\ 0 & \forall -\varepsilon_0 < \varphi_i < \varepsilon_0 \\ \varphi_i & otherwise \end{cases};\forall\varphi_i = \frac{1}{1+e^{a(q_{i,max}^{th}-q_i)(q_i-q_{i,min}^{th})/\Delta q_i^{th}}}, \forall a>0 \tag{8}$$

In general μ should be large enough to make the $1/w_i$ near to zero when JLA is activated, so that $\dot{q}_i \to 0$ as in this case $h(q_i)$ is bounded between ±1. In this case the role of $\bar{\varepsilon}$ is to

smoothen $h(q_i)$ when changes from φ_i to $-\varphi_i$. Away from the joint limits when $\varphi_i \approx 0$, w_i may still have oscillations due to large gain μ and oscillatory q_i, which is smoothened by implementing $\varepsilon_0 \approx 1e-4$.

The role of the term $(W_1 + W_2)^{-1} W_2$ in the null space of Jacobian needs to be discussed. Starting with $[W_2, W_1] \in I_{n \times n}$, if we increase W_1 (which will occur during JLA activation), keeping W_2 constant then since $\| W_1 \| \to \infty$, $\| (W_1 + W_2)^{-1} W_2 \| \to 0$ resulting diminishing contribution from null space. On the other hand, if we increase W_2, keeping W_1 constant, which will occur most of the time when the joint is away from its limits, $\| (W_1 + W_2)^{-1} W_2 \| \to 1$, since $(W_1 + W_2) \approx W_2$.

3. CONTROL SCHEMES AND STABILITY

Introducing Proportional (K_P) and Derivative (K_D) error control in Eq.(6) by positive definite diagonal gain matrices and task space error e $x_d - x = x_d - \kappa(q)$, we can arrive at the second order close loop kinematic scheme (Figure-1[a]) with error system [9][11][13][14]

$$\ddot{q} = J^h(\ddot{x}_d - \dot{J}\dot{q} + K_D\dot{e} + K_P e) + (I - J^h J)\xi_2; \quad \ddot{e} + K_D\dot{e} + K_P e = 0 \qquad (9)$$
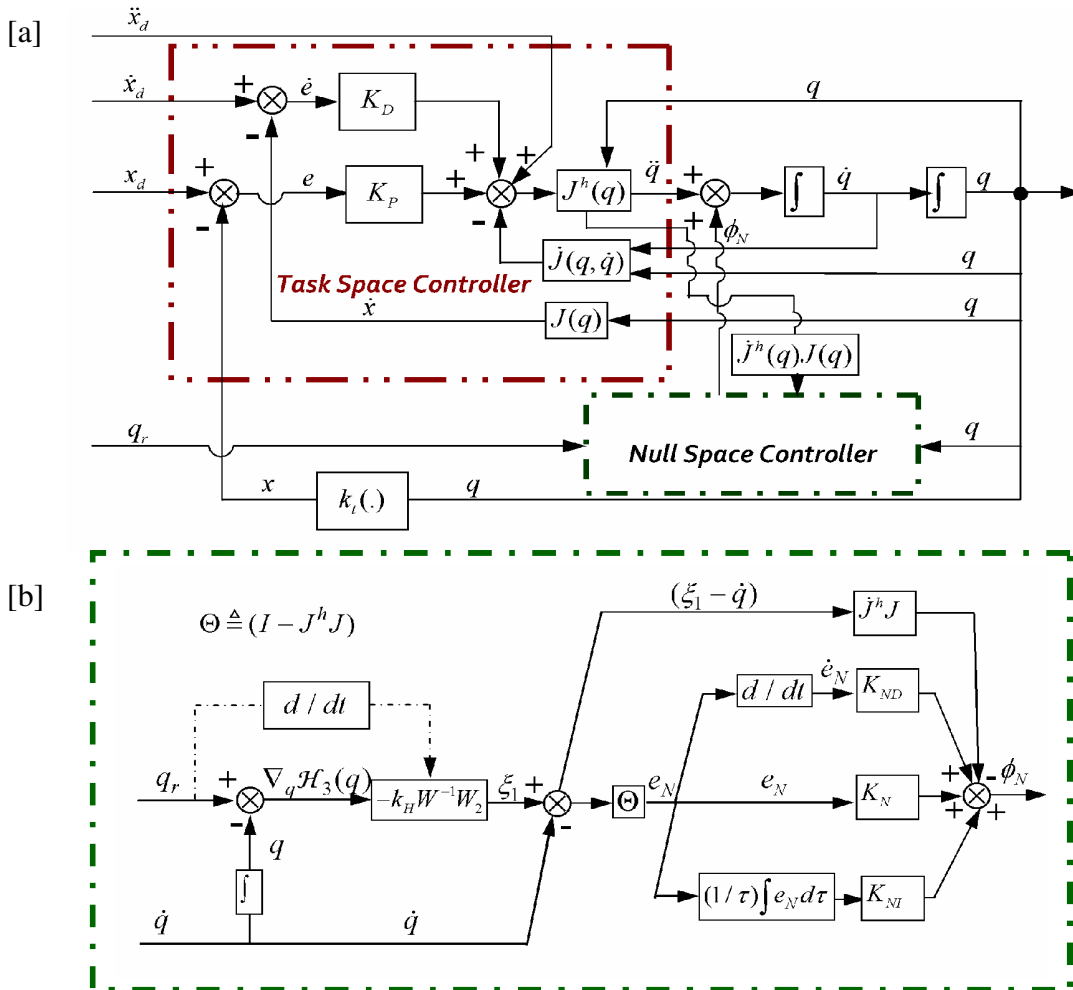
FIGURE 1: [a] Schematic implementation for 2nd order resolution in CWLS solution. [b] Null space controller schematic. ϕ_N is the null space contribution.

Continuous time stability can be analyzed by Lyapunov second or direct method for Eq.(9) by selecting Lyapunov candidate function $V(e) = (1/2)e^T Ke + V_2$, $\forall V(e) > 0$ and $V_2 = (1/2)\beta^2 \dot{q}^T K_{NS} \dot{q}$ resulting $\dot{V}(e) = e^T K\dot{e} + \dot{V}_2$. V_2 is included to ensure that the system does not go unstable in the Null Space Motion. K, K_{NS} are symmetric positive definite diagonal matrices for task space and null space respectively. Substituting the value of e and $\dot{e}$ in expression of $\dot{V}(e)$ and after simplification and substitution of $JJ^h = I$; and $J(I_{n \times n} - J^h J)\xi_1 = O$ we can establish $\dot{V}(e) = -e^T K^T K_p e + \dot{V}_2$. Considering the case of a constant reference $(\dot{x}_d = 0)$, the function $\dot{V}(e)$ is negative definite, under the assumption of full rank for J and β is so chosen such that $\dot{V}_2$ is negative, indicates solution is stable in Lyapunov sense. If we consider the regularized version [8] of CWLN solution, $\because JJ^{h*} \neq I$; $J(I - J^h J) = O$, and $(I - JJ^{h*}) \neq O$ the error system reduces to

$$\ddot{e} + K_D \dot{e} + K_P e = N[\ddot{x}_d - \dot{J}\dot{q} + K_D \dot{e} + K_P e]; \forall \mathbf{N} \quad (I - JJ^{h*}) \neq O \tag{10}$$

In defining the null space controller (Figure-1[b]), the first question that has to be answered is how many sub tasks the null space can simultaneously handle? If we choose k sub tasks each of rank r_k, the limit is $\sum_{i=1}^{k} r_i = n$. Once all the dof's are exhausted, it is useless to put additional low priority tasks, as their contribution will be always projected in to null space or they can even corrupt the primary task. Dropping the regularizing term for the time being and defining the null space error e_N, the null space contribution as ϕ_N is

$$\phi_N = (I - J^h J)[\dot{\xi}_1 + K_N e_N - \dot{J}^h J(\xi_1 - \dot{q})]; \forall e_N \quad (I - J^h J)(\xi_1 - \dot{q}) \tag{11}$$

Defining a Lyapunov positive definite candidate function $V(e_N) = (1/2)e_N^T e_N$, or $\dot{V}(e_N) = e_N^T \dot{e}_N$, substituting the values of $\dot{e}_N$ in $\dot{V}(e_N)$ and after simplification we can establish $\dot{V} = -K_N e_N^T e_N$, [Appendix-I.B] which is negative definite for positive definite symmetric null space proportional gain matrix K_N, which implies that the proposed controller in Eq.(11) stabilizes null space motion as long as the Jacobian is full rank.

4. RESULTS AND DISCUSSION

To illustrate the performance, we discuss the results of null space optimized $q_{cwls\_opt}(t)$ form in Eq.(6) and its canonical $q_{cwls\_ref}(t)$ form in Eq.(4), for a planar serial 3RRR manipulator following two distinct types of trajectories, namely, the trajectory resembling the motion of finger tip (Γ_1) and lamniscate trajectory (Γ_s). The particular solution $q_{cwls\_p}(t)$ and CWLN solution with joint limit activation $q_{cwls\_opt\_jla}(t)$ are also plotted to understand the contribution of null space and self motion.

In both the cases the link parameters in Denavit Hardenberg standard convention is $l_i = [1.5, 0.9, 0.7] cm$, $\alpha_i = [0,0,0], d_i = [0,0,0]$ and $\theta_i = [q_1, q_2, q_3]$. Γ_1 is analytically generated by joint space vector $q_t(t) = [0.3t^2 + 0.2; 0.5t^2 + 0.5; 0.7t^2 + 0.3]$ and the reference joint space vector is $q_r(t) = [0.4t + 0.2; 1.0t + 0.5; 1.0t + 0.5]$ with values far away from $q_t(t)$. JLA parameters in Eq.(8) are $\tau = 0.1$, $a = 100$, $\bar{\varepsilon} = 0.3$, $\varepsilon_0 = 1e-4$, $q_{max} = [0.8 \ 1.8 \ 2.6]^T$, $q_{min} = [-0.5 \ -0.5 \ -0.5]^T$, $\mu = 1e+7$. Initial values of $W_1 = I_{3 \times 3}$ and $W_2 = diag[45.0 \ 45.0 \ 45.0]$, resulting $(W_1 + W_2)^{-1} W_2 = 0.978$. The task space controller parameters are $K_P = diag[1 \ 1]*0.07/dt;$, $K_D = diag[1 \ 1]*0.9$ and

$K_I = diag[1\ 1] * 0.1$. The null space controller parameters are $k_H = 0.95$, $K_{NP} = diag[45\ 45\ 45]$, $K_{ND} = diag[4\ 4\ 4]$ and $K_{NI} = diag[10\ 10\ 10]$.

$q_{cwls\_opt}(t)$ solution for Γ_1 recovers the joint configuration better than $q_{cwls\_ref}(t)$ and it is in good agreement with $q_t(t)$ Figure-2[a]-[c]. The particular solution $q_{cwls\_p}(t)$ (range space) fails to follow $q_t(t)$ after $t \approx 0.5s$. The null space error e_N for q_1, rapidly converges from -0.7 at $t = 0s$ to -0.01 at $t = 0.02s$ and remains steady with a peak response at $t = 1.7s$ after which it again converges to zero (Figure-2[e]). The peak in e_N time history corresponds near configuration singularity in joint space between $1.3s \leq t \leq 1.7s$, in which σ_{min} (min svd(J)) drops from 1.2 to 0.56. The effect of $K_{ND}\dot{e}_N$ term is more prominent in contributing to ξ_2 and finally in null space acceleration ϕ_a.
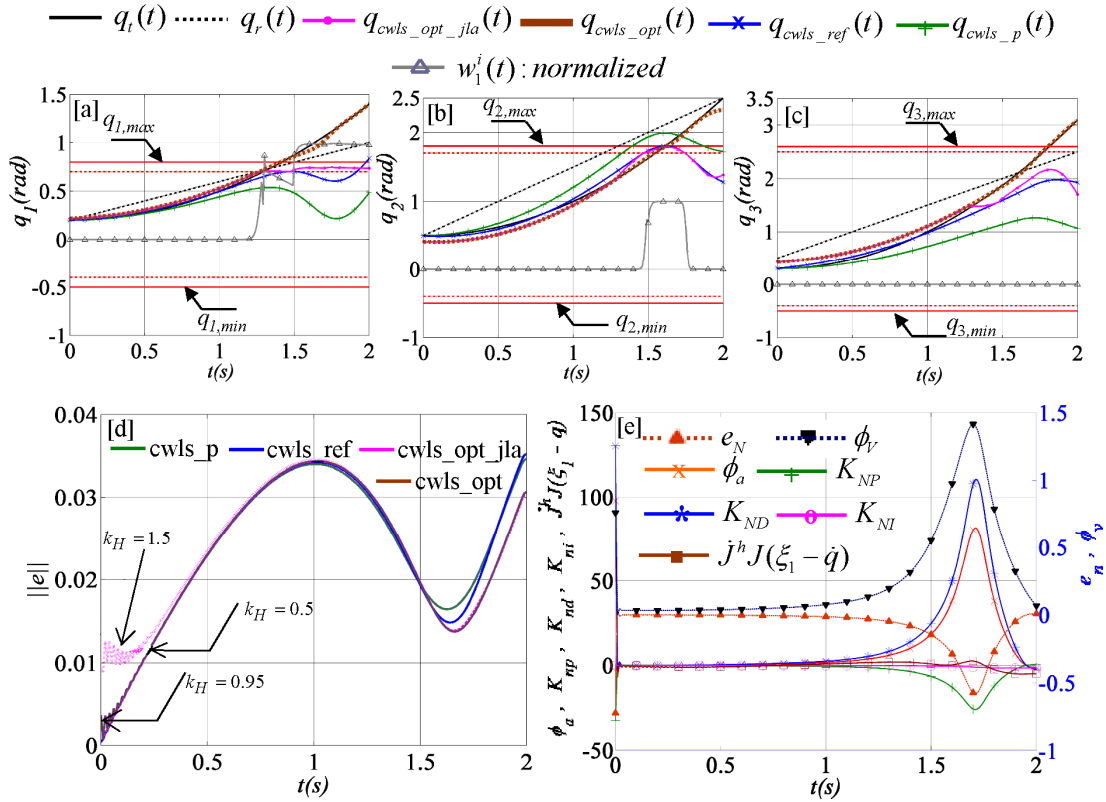
FIGURE 2: [a]-[c]: Time history of joint configurations with null space contribution for finger tip trajectory. Horizontal dotted lines represents joint activation threshold values q_{max}^{th} and q_{min}^{th} .[d] Time history of task space error norm $\|e(t)\|$.[e] Null space response for q_1 with out JLA, left Y-axis for variables e_N and null space velocity ϕ_V .

The contribution of $K_{NI}\frac{1}{\tau}\int e_N d\tau$ is insignificant here and contribution from $\dot{J}^h J(\xi_1 - \dot{q})$ is difficult to interpret in this case as its value is seen rising only during the configuration singularity period. The net effect of these terms is reflected in ϕ_a. Here ϕ_V is used to evaluate $\dot{q}(t)$ as a 1st order resolution and from which we can evaluate e_N and subsequently ϕ_a in the 2nd order resolution. Thus the null space interaction between $1.3s \leq t \leq 1.7s$, which raises ϕ_V and ϕ_a shifts the recovered joint space trajectory towards q_r and q_t in $q_{cwls\_opt}(t)$. This response can be utilized

for an event where some preferred poses are desired in joint space, keeping the task space error minimum. Increase in the value of the scalar k_H, results in initial oscillations in the solution as reflected in the Figure-2[d].

To observe the response of W_1 near joint limits, its normalized value is additionally plotted in Figure-2[a]-[c]. When q_1, reaches its joint threshold limit $q_{1,max}^{th} = 0.7 rad$, at $t = 1.26s$, the normalized value of w_1^1 in Eq.(8) increases from zero at $t = 1.17s$ to 0.6 at $t = 1.26s$. The first diagonal element of $(W_1 + W_2)^{-1} \to 0$, arresting further motion. The null space controller contribution is drastically scaled down as $(W_1 + W_2)^{-1} \to 0$, and the solution finally dominated by the particular solution. Arresting of motion near $q_{1,max}^{th}$ results oscillations in joint accelerations in second order formulation which amplifies oscillations in φ^1, by the term μ. This is because we have formulated the JLA algorithm based on the joint configuration as $\varphi_t = f(q_t, q_{max}^{th}, q_{max}, q_{min}^{th}, q_{min})$. This will only occur when q_1 over shoots $q_{1,max}^{th}$ in k^{th} time step gets damped and returned back to lower value in $(k+1)^{th}$ time step, until it is gradually damped out. This behavior has been reduced by implementing the term ε_0 in Eq.(8). For joint 2, the $q_{cwls\_p}(t)$ solution overshoots the limit and $q_{cwls\_ref}(t)$ touches the maximum limit. For joint 3, JLA is not actuated for $q_{cwls\_opt}(t)$ as it is well under actuation threshold limit.

For the Regularized Composite Least Square (RCWLS) solution, the lamniscate trajectory (Γ_s) simulates the condition of reaching workspace singularity condition, crossing it and then moving away form it as the trajectory is closed and has two distinct lobes which results in multimodal joint space trajectories. Moreover this particular case is extreme as $q_t(t)$ and $q_r(t)$ differs both in amplitude and phase. The iteration started with $W_1 = I_{3\times3}$, $W_2 = diag[75.0\ 75.0\ 75.0]$, $q_{i,min} = [-1.5\ -0.5\ -0.5]$, $q_{i,max} = [2\ 2.3\ 2.3]$, $\tau = 0.25\ rad$, $a = 75$; $\bar{\varepsilon} = 0.4$; $\varepsilon_0 = 1e-4$; $\mu = 1e+7$, $K_P = diag[45\ 45]$, $K_D = diag[0.45\ 0.45]$, and $K_I = diag[0.1\ 0.1]$. The null space controller parameters are $k_H = 0.95$, $K_{NP} = diag[45\ 45\ 45]$, $K_{ND} = diag[2.5\ 2.5\ 2.5]$, and $K_{NI} = diag[1.0\ 1.0\ 1.0]$.

The first workspace singularity crossing occurs between $0.08s \leq t \leq 0.3s$ when the tip crosses from A to B in Γ_s (Figure-3[d]) and second workspace singularity occurs between $1.1s \leq t \leq 1.5s$ when the tip crosses from C to D. In between these two, the solution faces near configuration singularity when it crosses from P to Q between $0.6s \leq t \leq 0.8s$ and from R to S between $1.6s \leq t \leq 1.8s$. It is to be mentioned here that initial high oscillating acceleration between $0.0s \leq t \leq 0.05s$ in $\|e\|$ is due to the task space gains. In the near configuration singularity cases (pq and rs) in Figure-3[e] which lowers $\sigma_m(t)$ between $0.6s \leq t \leq 0.8s$ and $1.6s \leq t \leq 1.8s$, the damping parameter $\alpha(t)$ does not interfere $\forall \varepsilon = 0.5$, the threshold value to initiate damping and $\alpha(t) = f(\sigma_m, \varepsilon)$.

$q_{cwls\_opt\_jla}(t)$ solution increased $\|e\|$ between $1.3s \leq t \leq 1.5s$ due to the simultaneous occurrences of JLA for q_3 and singularity crossings from C to D. It should be noted that in the expression of $J^{h*} = (W_1 + W_2)^{-1} J^T (J(W_1 + W_2)^{-1} J^T + \alpha^2 I_{m\times m})^{-1}$, increase of $\alpha(t)$ to α_{max} during singularity keeping $W_1\ and\ W_2$ to its initial values, will reduce the over all value of J^{h*}. On the contrary, during JLA, increase of the diagonal element $w_{1,3}$ of the weighing matrix W_1 to a very high value (Oe+7), will only make the third row of J^{h*} approaching to zero in order to make that

particular joint immobile but the other two rows of J^{h*} may increase or decrease as per the action of the task space controller.

So the combined effect is overall damping of J^{h*} due to $\alpha(t)$ and the third row is approaching zero. This increases the task space error between $1.3s \leq t \leq 1.5s$ in comparison to $q_{cwls\_opt}(t)$, where only singularity avoidance is active. The null space contribution from $(\phi_v \ and \ \phi_a)$ has been considerably diminished as high gain of W_1 during JLA makes $(W_1 + W_2)^{-1} \to 0$ and W_2 remains constant in the null space. Further increase of value of $W_2 \ and \ k_H$ and null space gain parameters results in increased oscillation in initial joint velocity and acceleration and also increases $\parallel e \parallel$. The task space and null space gains are kept on the higher side in the simulation which causes initial oscillations in joint space in some cases. It has been verified that reducing these gains eliminates these initial oscillations except during near singular or singularity crossings. The role of the weighing matrices $W_1 \ and \ W_2$ has been defined with a bias to higher gain of W_2 which will amplify the null space contribution and in doing this the $(W_1 + W_2)^{-1}W_2$ term is advantageously used.
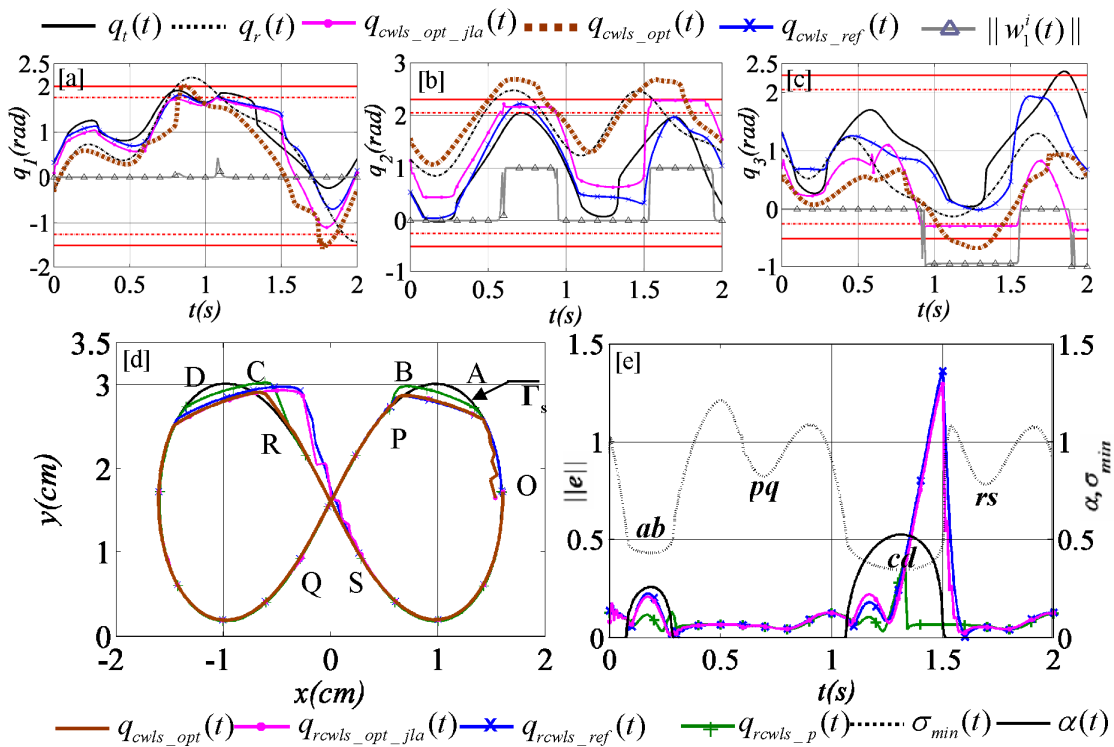
FIGURE 3: [a]-[c]: Time history of joint configurations with null space contribution for lamniscate trajectory Γ_s. Horizontal dotted lines represents joint activation threshold values q_{max}^{th} and q_{min}^{th} .[d] Trajectory trace for the solutions. Analytical trajectory generating workspace singularity Γ_s is OABPQDCRSO. [e] Time histories for $\parallel e \parallel$, α and $\sigma_m \quad min \ svd(J)$ values.

In a hypothetical situation, we want to see the response when the reference signal (q_r) in joint space approximates the analytical joint trajectory $(q_r = 0.9q_t)$, as in the earlier cases q_r is generated with considerably deviation from q_t. For trajectory Γ_1, (Figure-4: Top row) both

$q_{cwls\_opt}(t)$ and $q_{cwls\_ref}(t)$ solutions remain in between q_t and q_r, and the difference between them can be neglected where as the particular solution deviates significantly q_t as before.

Similar responses obtained from trajectory Γ_s for lamniscate path (Figure-4: Bottom row) for $q_r = 0.9 q_t$. In this situation, the null space error e_N, for trajectory Γ_1, remains stable at ≈ 0 until it briefly oscillates in near configuration singularity period between $1.3s \le t \le 1.7s$ (Figure-5: Left) and between $0.6s \le t \le 0.7s$ and $1.5s \le t \le 1.7s$ for lamniscate trajectory Γ_s (Figure-5: Right). During these time periods there is a surge in ϕ_V and ϕ_a injecting the null space contribution in the solution. For the remaining time in all cases, the null space contribution is ≈ 0, which is desired as the recovered joint space trajectory is in between q_t and q_r (Figure-4: Top Row).
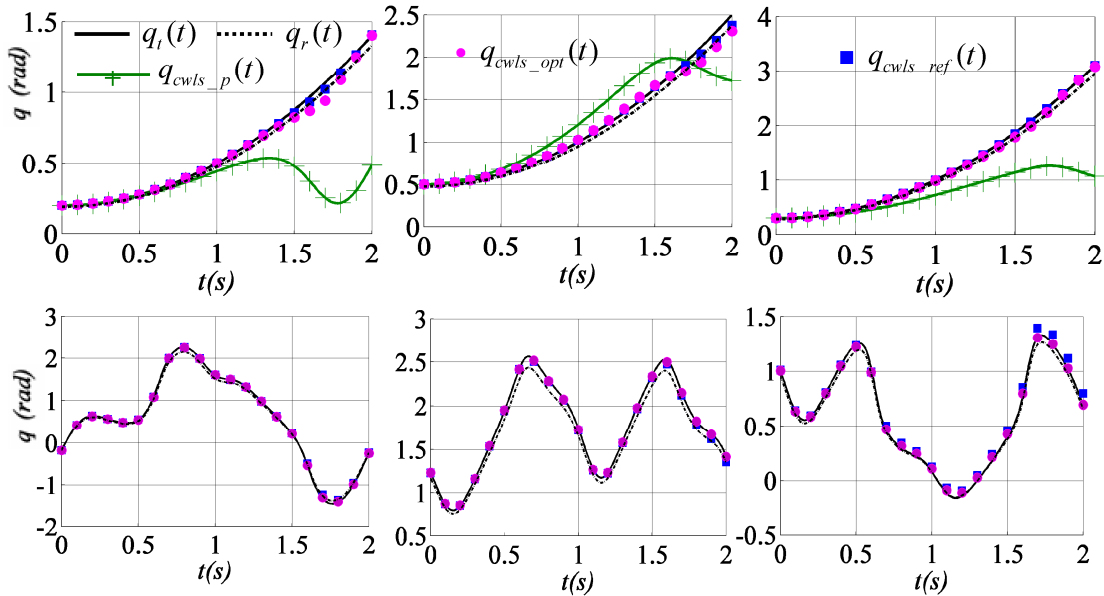
FIGURE 4: Top: Time history of joint configurations for trajectory Γ_1 with the special case of $q_r = 0.9 q_t$. Bottom: Time history of joint configurations for trajectory Γ_s with the special case of $q_r = 0.9 q_t$. All results are for $q_{cwls\_opt}(t)$ solution. Columns from left represent joints q_1, q_2 and q_3 respectively.
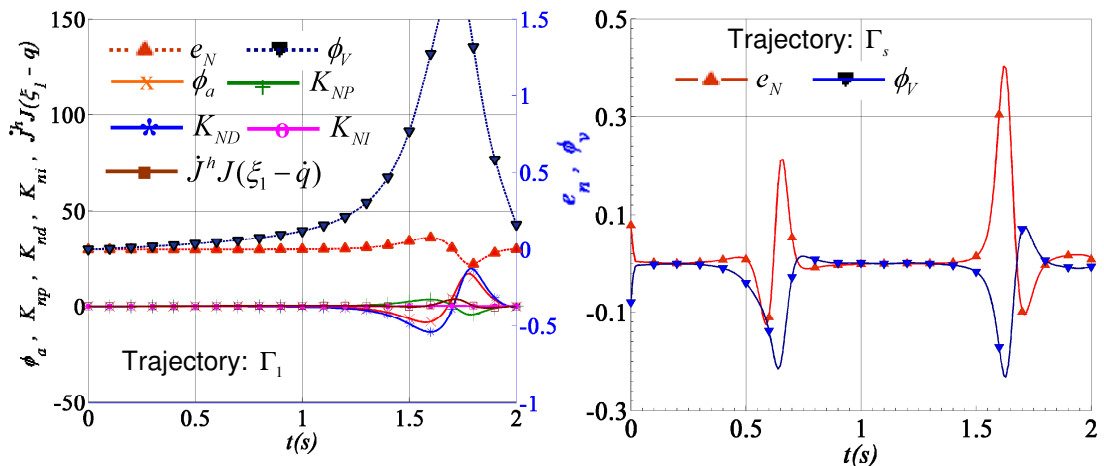
FIGURE 5: Left : Null space response for Γ_1 when $(q_r = 0.9 q_t)$ Left Y-axis for variables e_N and ϕ_V. Right: Null space response for variables e_N and ϕ_V for lamniscate trajectory Γ_s. All results are for $q_{cwls\_opt}(t)$ solution.

5. CONCLUSION

By composite weighting the range and null space we can arrive at a solution which is able to handle both joint limits and preferred joint configuration, simultaneously satisfying the primary task. The solution lies between q_t and q_r also shifts the recovered joint space to wards the reference configuration q_r without JLA. In this formulation the role of W_2 and q_r is of paramount importance as it controls the contribution form null space along with scalar k_H. It has been observed that null space velocities ϕ_V and acceleration ϕ_a are shooting up antagonistically to e_N which signifies that the null space controller is working and there is self motion contribution form null space when e_N is facing a drift from asymptotic stability. This enables the CWLS framework to retrieve the desired joint configuration given the desired task space and preferred joint rate $(\dot{q}_r)$ without considering any joint dependency.

The response can be utilized for an event where some preferred poses are desired in joint space, keeping the task space error minimum, which can be exploited for recovering various human postures where the motion workspace is limited and there is practical difficulty in mounting optical markers or inertial motion sensors due to limited space availability or hindrance in natural articulation. A typical application in this regard is recovering human palmer grasps (full closure of fist) postures which are currently under study. The task is challenging, as in human palmer grasp motion, apart from it's high dimensionality, the problem is much more aggravated by limited workspace space availability, cross finger occlusion, constraints in finger joint motion and full traversal of joint motion ranges. The state of the art motion tracking technologies using optical or inertial sensing for retrieving position and orientation data from each joint sometimes becomes infeasible for this particular grasp mode, due to space limitations and slip, which results in restricting natural articulation.

The limitation with $(W_1+W_2)^{-1}$ term is with the activation of JLA, it reduces the null space contribution. Sensitivity of k_H parameter is another issue and hence its bound has been kept in between 0.75-0.95 for most of the cases as it is additionally coupled with the term $(W_1+W_2)^{-1}W_2$. The other important limitation observed in CWLS scheme is its dependency on initial configuration. Hence it will require an initial configuration close to the analytical solution.

6. REFERENCES

[1] A. Liëgeois. "Automatic supervisory control of the configuration and behavior of multibody mechanisms." IEEE Transactions on Systems, Man, and Cybernetics, SMC-vol.7(12), pp.868–871, 1977.

[2] N. Mansard and F. Chaumette. "Directional redundancy for robot control." IEEE Transactions on Automatic Control, vol.54(6), pp.1179–1192, 2009.

[3] T. F. Chan and R. V. Dubey. "A weighted least-norm solution based scheme for avoiding joint limits for redundant joint manipulators." IEEE Transactions on Robotics and Automation, vol.11(2), pp. 286–292, 1995.

[4] F. Chaumette, E. Marchand. "A redundancy-based iterative approach for avoiding joint limits: Application to visual servoing." IEEE Trans. On Robotics and Automation, vol.17(5), pp.719-730, October 2001.

[5] Y. Nakamura, H. Hanafusa, T. Yoshikawa, "Task-Priority Based Control of Robot Manipulators." International Journal of Robotics Research, vol. 6(2), pp. 3 - 15, 1987.

[6]   Oussama Kanoun, Florent Lamiraux, Pierre-Brice Wieber. "Kinematic Control of Redundant Manipulators: Generalizing the Task-Priority Framework to Inequality Task." IEEE Transactions on Robotics vol.27(4), pp. 785-792, 2011.

[7]   J. Baillieul. "Avoiding obstacles and resolving kinematic redundancy. In Proceedings of IEEE International Conference on Robotics and Automation, Washington, UWA, 1986, pp 1698–1704.

[8]   G. Antonelli. "Stability analysis for prioritized closed-loop inverse kinematic algorithms for redundant robotic systems," IEEE Trans. Robot., vol. 25(5), pp. 985–994, Oct. 2009.

[9]   Hsu, P., Hauser, J. and Sastry, S. "Dynamic control of redundant manipulators." Journal of Robotic Systems, vol.6(2), pp. 133–148, 1989.

[10]   Senda, K. "Quasioptimal control of space redundant manipulators." AIAA Guidance, Navigation, and Control Conference, 1999, pp. 1877–1885.

[11]   Bojan Nemec and Leon Zlajpah, " Null space velocity control with dynamically consistent pseudo-inverse." Robotica, vol.18, pp. 513–518, 2000.

[12]   Tsuyoshi Shibata and Toshiyuki Murakami, "Null Space Motion Control by PID Control Considering Passivity in Redundant Manipulator." IEEE Trans. on Industrial Informatics, vol. 4(4), pp.261-270, November 2008.

[13]   G. Antonelli, F. Arrichiello, S.Chiaverini. "The null-space-based behavioral control for autonomous robotic systems." Intel Serv Robotics, vol.1, pp.27–39, 2008.

[14]   J.Nakanishi, R. Cory, M. Mistry, J. Peters and S. Schaal. "Operational Space Control: A Theoretical and Empirical Comparison." The International Journal of Robotics Research, vol.27(6), pp. 737-757, 2008.

APPENDIX- I.A CWLS derivation

Objective : $min(\dot{q})\mathsf{H}_3(\dot{q}) = min(\dot{q})[(1/2)\dot{q}^T W_1 \dot{q} + (1/2)(\dot{q} - \dot{q}_r)^T W_2(\dot{q} - \dot{q}_r)]; \; s.t \; J\dot{q} = \dot{x}$

$\forall (W_1, W_2) \in \;^{n \times n}$ and positive diagonal positive definite ,

$Lagrangian : L(\dot{q}, \lambda) = \mathsf{H}(\dot{q}) + \lambda(J\dot{q} - \dot{x}) = [(1/2)\dot{q}^T W_1 \dot{q} + (1/2)(\dot{q} - \dot{q}_r)^T W_2(\dot{q} - \dot{q}_r)] + \lambda(J\dot{q} - \dot{x})$

$\nabla_{\dot{q}} L = \dfrac{\partial L^T}{\partial \dot{q}} \Rightarrow W_1 \dot{q} + W_2(\dot{q} - \dot{q}_r) + J^T \lambda = 0 \; and \;\; \nabla_\lambda L = J\dot{q} - \dot{x} = 0 \; with \; \nabla_{\dot{q}}^2 L = (W_1 + W_2) > 0$

$\Rightarrow W_1 \dot{q} + W_2(\dot{q} - \dot{q}_r) + J^T \lambda = 0 \;\; \Rightarrow (W_1 + W_2)\dot{q} = W_2 \dot{q}_r - J^T \lambda; \;\; \Rightarrow \dot{q} = (W_1 + W_2)^{-1}(W_2 \dot{q}_r - J^T \lambda)$

$Putting \; the \; value \; of \; \dot{q} \; in \; \nabla_\lambda L = 0; \; J(W_1 + W_2)^{-1}(W_2 \dot{q}_r - J^T \lambda) \; = \dot{x};$

$\Rightarrow \lambda \; = (J(W_1 + W_2)^{-1} J^T)^{-1}[J(W_1 + W_2)^{-1} W_2 \dot{q}_r - \dot{x}] \; and \; \forall W \;\;\; (W_1 + W_2), \lambda \; = (JW^{-1} J^T)^{-1}[JW^{-1} W_2 \dot{q}_r - \dot{x}]$

$\Rightarrow \dot{q} = W^{-1} J^T (JW^{-1} J^T)^{-1} \dot{x} + (I - W^{-1} J^T (JW^{-1} J^T)^{-1} J)W^{-1} W_2 \dot{q}_r$

$\forall \, J^\hbar \;\;\; W^{-1} J^T (JW^{-1} J^T)^{-1}; \forall \xi_1 \;\;\; (W_1 + W_2)^{-1} W_2 \dot{q}_r;$

Avik Chatterjee, S. Majumder & I. Basak

$$\dot{q} = J^{\hbar}\dot{x} + (I - J^{\hbar}J)(W_1 + W_2)^{-1}W_2\dot{q}_r = J^{\hbar}\dot{x} + (I - J^{\hbar}J)\xi_1$$

APPENDIX- I.B Null space Lyapunov stability.

Differentiating the null space error term e_N in Eq.(11),

$$\dot{e}_N = (I - J^{\hbar}J)(\dot{\xi}_1 - \ddot{q}) - (\dot{J}^{\hbar}J + J^{\hbar}\dot{J})(\xi_1 - \dot{q}) \ ;$$

rewriting $(\xi_1 - \dot{q})$ and substituting in $\dot{e}_N$,

$$\dot{e}_N = (I - J^{\hbar}J)(\dot{\xi}_1 - \ddot{q}) - \dot{J}^{\hbar}Je_N - J^{\hbar}\dot{j}e_N - (\dot{J}^{\hbar}JJ^{\hbar} + J^{\hbar}\dot{J}J^{\hbar})J(\xi_1 - \dot{q}); \ \because Je_N = 0 \ as \ e_N \in \ (J), \ and$$

$JJ^{\hbar} = I, \ \Rightarrow \dot{J}J^{\hbar} + J\dot{J}^{\hbar} = 0$; which after simplification

$$\dot{e}_N = (I - J^{\hbar}J)(\dot{\xi}_1 - \ddot{q}) - J^{\hbar}\dot{j}e_N - (I - J^{\hbar}J)\dot{J}^{\hbar}J(\xi_1 - \dot{q})$$

Now $(I - J^{\hbar}J)\dot{J}^{\hbar}J(\xi_1 - \dot{q}) = (I - J^{\hbar}J)(\dot{\xi}_1 + K_N e_N) - \phi_N$ from Eq. (11)

$$or, \dot{e}_N = (I - J^{\hbar}J)(\dot{\xi}_1 - \ddot{q}) - J^{\hbar}\dot{j}e_N - (I - J^{\hbar}J)\dot{\xi}_1 - (I - J^{\hbar}J)K_N e_N + \phi_N$$

Substituting the value of $\ddot{q}$ from Eq.(6)

$$\dot{e}_N = (I - J^{\hbar}J)[(\dot{\xi}_1 - J^{\hbar}((\ddot{x}_d - \dot{J}\dot{q}) + \ddot{q}_N)] - J^{\hbar}\dot{j}e_N - (I - J^{\hbar}J)\dot{J}^{\hbar}J(\xi_1 - \dot{q})]$$

$$= (I - J^{\hbar}J)\dot{\xi}_1 - (I - J^{\hbar}J)J^{\hbar}(\ddot{x}_d - \dot{J}\dot{q}) - (I - J^{\hbar}J)\ddot{q}_N - J^{\hbar}\dot{j}e_N - (I - J^{\hbar}J)\dot{J}^{\hbar}J(\xi_1 - \dot{q})$$

$$= (I - J^{\hbar}J)\dot{\xi}_1 - (I - J^{\hbar}J)\ddot{q}_N - J^{\hbar}\dot{j}e_N - (I - J^{\hbar}J)\dot{\xi}_1 - (I - J^{\hbar}J)K_N e_N + \phi_N$$

$$= -J^{\hbar}\dot{j}e_N - (I - J^{\hbar}J)K_N e_N; \ \because (I - J^{\hbar}J)\ddot{q}_N \ projects \ \ddot{q}_N \ in \ N(J) \ and \ = \phi_N$$

$$\therefore \dot{e}_N = -(I - J^{\hbar}J)K_N e_N - J^{\hbar}\dot{j}e_N \ .$$

Defining a Lyapunov positive definite candidate function :

$$V = (1/2)e_N^T e_N \Rightarrow \dot{V} = e_N^T \dot{e}_N \text{ and substituting the values of } \dot{e}_N$$

$$\dot{V} = e_N^T(-(I - J^{\hbar}J)K_N e_N - J^{\hbar}\dot{j}e_N) = -e_N^T(I - J^{\hbar}J)K_N e_N - e_N^T J^{\hbar}\dot{j}e_N)$$

$$= -e_N^T K_N e_N + e_N^T J^{\hbar}JK_N e_N - e_N^T J^{\hbar}\dot{j}e_N = -K_N e_N^T e_N + e_N^T J^{\hbar}(K_N J - \dot{J})e_N$$

$$\because e_N^T J^{\hbar} = [(I - J^{\hbar}J)(\xi_1 - \dot{q})]^T J^{\hbar} = (\xi_1 - \dot{q})^T(I - J^{\hbar}J)^T J^{\hbar} = (\xi_1 - \dot{q})^T(I - J^{\hbar}J)J^{\hbar} = 0$$

$$\Rightarrow \dot{V} = -K_N e_N^T e_N$$

which is negative definite for positive definite symmetric null space proportional gain matrix K_N, which implies that the proposed controller stabilizes null space motion as long as the Jacobian is full rank.

INSTRUCTIONS TO CONTRIBUTORS

Robots are becoming part of people's everyday social lives - and will increasingly become so. In future years, robots may become caretaking assistants for the elderly or academic tutors for our children, or medical assistants, day care assistants, or psychological counselors. Robots may become our co-workers in factories and offices, or maids in our homes.

The International Journal of Robotics and Automation (IJRA), a refereed journal aims in providing a platform to researchers, scientists, engineers and practitioners throughout the world to publish the latest achievement, future challenges and exciting applications of intelligent and autonomous robots. IJRA is aiming to push the frontier of robotics into a new dimension, in which motion and intelligence play equally important roles. IJRA scope includes systems, dynamics, control, simulation, automation engineering, robotics programming, software and hardware designing for robots, artificial intelligence in robotics and automation, industrial robots, automation, manufacturing, and social implications.

To build its International reputation, we are disseminating the publication information through Google Books, Google Scholar, Directory of Open Access Journals (DOAJ), Open J Gate, ScientificCommons, Docstoc and many more. Our International Editors are working on establishing ISI listing and a good impact factor for IJRA.

The initial efforts helped to shape the editorial policy and to sharpen the focus of the journal. Started with Volume 4, 2013, IJRA appears with more focused issues. Besides normal publications, IJRA intends to organize special issues on more focused topics. Each special issue will have a designated editor (editors) – either member of the editorial board or another recognized specialist in the respective field.

We are open to contributions, proposals for any topic as well as for editors and reviewers. We understand that it is through the effort of volunteers that CSC Journals continues to grow and flourish.

IJRA LIST OF TOPICS
The realm of International Journal of Robotics and Automation (IJRA) extends, but not limited, to the following:

- Automation Control
- Autonomous Robots
- Emergence of The Thinking Machine
- Household Robots and Automation
- Jacobian and Singularities
- Nanotechnology & Robotics (Nanobots)
- Robot Controller
- Robotic & Automation Software Development
- Robotic Surgery
- Robotic Welding
- Robotics Programming
- Robots Society and Ethics

- Spatial Transformations
- Unmanned (Robotic) Vehicles

- Automation Engineering
- Biotechnology & Robotics
- Forward Kinematics
- Inverse Kinematics
- Methods for Teaching Robots
- Orientation Matrices
- Robot Structure and Workspace
- Robotic Exploration

- Robotic Surgical Procedures
- Robotics Applications
- Robotics Technologies
- Software and Hardware Designing for Robots
- Trajectory Generation

CALL FOR PAPERS

Volume: 4 - **Issue: 2**

i. Paper Submission: September 30, 2013   **ii. Author Notification:** October 31, 2013

iii. Issue Publication: November 2013

CONTACT INFORMATION